Inorg. Chem. **2007**, *46*, 3257–3274

Spin Exchange Effects on the Physicochemical Properties of Tetraoxolene-Bridged Bimetallic Complexes

Dong Guo and James K. McCusker*

Department of Chemistry, Michigan State University, East Lansing, Michigan 48824

Received January 2, 2007

The synthesis, physical, and spectroscopic properties of a series of metal complexes bridged by the redox-active chloranilate ligand are described. Compounds containing the $(CA^{cat,cat})^{4-}$ ligand, where $(CA^{cat,cat})^{4-}$ represents the fully reduced aromatic form of chloranilate, have been prepared by two different routes from H_2CA and H_4CA starting materials; the corresponding $(CA^{sq,cat})^{3-}$ analogue was obtained by one-electron oxidation with decamethylferrocenium tetrafluoroborate. Homo- and heterobimetallic complexes containing Cr^{III} and Ga^{III} with chloranilate have been prepared, yielding the following six complexes: $[Ga_2(tren)_2(CA^{cat,cat})](BPh_4)_2$ (**1**), $[Ga_2(tren)_2(CA^{sq,cat})](BPh_4)_2(BF_4)$ (**2**), $[GaCr(tren)_2(CA^{cat,cat})](BPh_4)_2$ (**3**), $[GaCr(tren)_2(CA^{sq,cat})](BPh_4)_2(BF_4)$ (**4**), $[Cr_2(tren)_2(CA^{cat,cat})](BPh_4)_2$ (**5**), and $[Cr_2(tren)_2(CA^{sq,cat})](BPh_4)_2(BF_4)$ (**6**) (where tren is tris(2-aminoethyl)amine). Single-crystal X-ray structures have been obtained for complexes **1**, **3**, and **5**; nearly identical C–C bond distances within the quinoidal ligand confirm the aromatic character of the bridge in each case. Complex **2** exhibits a temperature-independent magnetic moment of $\mu_{eff} = 1.64 \pm 0.04\ \mu_B$ in the solid state between 4 and 350 K, consistent with the $CA^{sq,cat}$ formulation of the ligand and an $S = 1/2$ ground state for complex **2**. Complex **3** exhibits a value of $\mu_{eff} = 3.44 \pm 0.09\ \mu_B$ that is also temperature-independent, indicating an $S = 3/2$ ground state. Complexes **4**–**6** are all influenced by Heisenberg spin exchange. The temperature-independent behavior of complexes **4** and **6** indicate the presence of strong antiferromagnetic exchange between the Cr^{III} and the (sq,cat) bridging radical yielding well-isolated ground states of $S = 1$ and 5/2 for **4** and **6**, respectively. In contrast, complex **5** exhibits a weak intramolecular antiferromagnetic exchange interaction between the two Cr^{III} centers ($J = -2\ cm^{-1}$ for $\hat{H} = -2J\hat{S}_1 \cdot \hat{S}_2$) via superexchange through the diamagnetic $CA^{cat,cat}$ bridge. The absorption spectra of the $CA^{sq,cat}$-containing complexes exhibit a number of sharp, relatively intense features in fluid solution. Group theoretical arguments coupled with a qualitative ligand-field analysis including the effects of Heisenberg spin exchange suggest that several of the observed transitions are a consequence of exchange interactions in both the ground- and excited-state manifolds of the compounds.

Introduction

Interest in exchange coupling is expanding from its origins in fundamental electronic structure research to encompass a variety of disciplines ranging from biology to materials science.[1−11] For example, the occurrence of polynuclear metal clusters at the active sites of metalloproteins demands an understanding of exchange effects both for the characterization of the electronic structures of these types of proteins, as well as assessing its possible role in chemical reactivity.[12−23]

* To whom correspondence should be addressed. E-mail: jkm@cem.msu.edu.

(1) Hendrickson, D. N. *Research Frontiers in Magnetochemistry*; O'Connor, C. J., Ed.; World Scientific: Singapore, 1993.
(2) Kahn, O. *Molecular Magnetism*; VCH Publishers: New York, 1993.
(3) Kahn, O. *Acc. Chem. Res.* **2000**, *33*, 647.
(4) Beltran, L. M. C.; Long, J. R. *Acc. Chem. Res.* **2005**, *38*, 325 and references therein.
(5) Holm, R. H.; Kennepohl, P.; Solomon, E. I. *Chem. Rev.* **1996**, *96*, 2239−2314.
(6) *Magnetic Molecular Materials*; Gatteschi, D., Kahn, O., Miller, J. S., Palacio, F., Eds.; Kluwer Academic Publishers: Dordrecht, The Netherlands, 1991; Vol. 198.
(7) Yoon, J.; Mirica, L. M.; Stack, T. D. P.; Solomon, E. I. *J. Am. Chem. Soc.* **2004**, *126*, 12586.
(8) Yoon, S.; Lippard, S. J. *J. Am. Chem. Soc.* **2005**, *127*, 8386.
(9) Moragues-Cánovas, M.; Rivière, É.; Ricard, L.; Paulsen, C.; Wernsdorfer, W.; Rajaraman, G.; Brechin, E. K.; Mallah, T. *Adv. Mater.* **2004**, *16*, 1101.
(10) Stamatatos, T. C.; Foguet-Albiol, D.; Stoumpos, C. C.; Raptopoulou, C. P.; Terzis, A.; Wernsdorfer, W.; Perlepes, S. P.; Christou, G. *J. Am. Chem. Soc.* **2005**, *127*, 15380.
(11) Shultz, D. A.; Fico, R. M., Jr.; Bodnar, S. H.; Kumar, R. K.; Vostrikova, K. E.; Kampf, J. W.; Boyle, P. D. *J. Am. Chem. Soc.* **2003**, *125*, 11761.

10.1021/ic070005y CCC: $37.00 © 2007 American Chemical Society
Published on Web 03/20/2007

Recent interest in the development of molecular magnets[24] is based on the notion of exploiting spin exchange interactions to yield compounds that exhibit bulklike magnetic behavior at the single-molecule level. In these and many other contexts, an understanding of the cause-and-effect relationship between spin exchange and the physicochemical properties of molecular systems is critical for the rational design of complex spin-coupled assemblies.

In this regard, metal−quinone complexes represent a convenient platform for studying the physicochemical properties of exchange-coupled molecules. The redox activity of the quinone ligand provides an effective mechanism for turning "on" or "off" electron exchange, thereby allowing one to probe the effects of spin coupling in closely related sets of chemical systems. Over the past two decades, the study of transition metal−quinone compounds has developed into a rich field in terms of both synthetic and physical chemistries.[25−33] From the perspective of electronic structure theory, transition metal−semiquinone complexes are the most interesting owing to the radical nature of the semiquinone ligand, which produces compounds with unusual magnetic and optical properties[34−36] that appear to be governed by interactions arising between unpaired electrons localized on the metal and the bound organic radical.[37−39] Chelating tetraoxolenes have attracted attention in part because of their non-innocent behavior (i.e., reversible redox chemistry),[40−48] as well as their ability to act as a bridging unit for the preparation of multinuclear assemblies.[49] The ligand-based redox activity associated with this substrate is illustrated in Scheme 1. When combined with paramagnetic transition metals, tetraoxolene complexes can exhibit exceptionally rich electrochemical, magnetic, and spectroscopic behavior.

Due in part to the small energy gap between tetraoxolene π^* and transition metal d orbitals,[50] variability with respect to the tetraoxolene and/or metal oxidation states are a complicating feature of these systems. Dinuclear complexes containing a variety of first-row metal ions (Cu^{II}, Ni^{II}, Fe^{III}, and Cr^{III})[51−55] appear to have a rather localized charge distribution with the oxidation state of bridging ligand being assigned as the dianionic form (sq,sq); analogous descriptions have been also proposed for the $[(cod)Rh^{I}(CA^{sq,sq})Rh^{I}(cod)]$ complex (cod = cycloocta-1,5-diene)[46] and $[Mo_2(DAniF)_3]_2(C_6X_2O_4)$ (X = H, Cl, or NO_2).[47] In contrast, the dimeric complex $[Co_2(DHBQ)(tdpme)_2](BF_4)_2\cdot CH_2Cl_2$ (where dhbq = 2,5-dihydroxy-1,4-benzoquinone and tdpme = 1,1,1-tris(diphenylphosphanomethyl)ethane)[51] exhibits C−O bond distances longer than those of the free ligand $dhbq^{2-}$, suggesting more single-bond character to these bonds and a (cat,cat) description for the ligand. The radical (sq,cat) form appears to be realized in an iron complex of two tetraazamacrocycle complexes $[Fe_2(DHBQ)_2(CTH)_2]Y\cdot nH_2O$ (CTH = 5,7,7,12,14,14-hexamethyl-1,4,8,11-tetraazacyclodecane, Y = ClO_4^-, PF_6^-),[56] the chromium complex $[Cr_2(CTH)_2(DHBQ)Y_3$ (Y = ClO_4^-, PF_6^-),[56] and the cobalt-containing system $[Co_2(CTH)_2(dhbq)](PF_6)_3$.[43] Miller and coworkers have reported the crystal structure and magnetic properties of $[(TPA)Co^{II}(CA^{sq,cat})Co^{II}(TPA)](BF_4)$.[57a] The chloranilate bridge, which we are also employing in our study, is formulated as (sq,cat) in this system as well, with both cobalt ions in high-spin divalent configurations; this

(12) Achim, C.; Bominaar, E. L.; Staples, R. J.; Münck, E.; Holm, R. H. *Inorg. Chem.* **2001**, *40*, 4389 and references therein.
(13) Weldon, B. T.; Wheeler, D. E.; Kirby, J. P.; McCusker, J. K. *Inorg. Chem.* **2001**, *40*, 6802.
(14) Picraux, L. B.; Smeigh, A. L.; Guo, D.; McCusker, J. K. *Inorg. Chem.* **2005**, *44*, 7846.
(15) Picraux, L. B.; Weldon, B. T.; McCusker, J. K. *Inorg. Chem.* **2003**, *42*, 273.
(16) Bertrand, P.; Gayda, J.-P. *Biochim. Biophys. Acta* **1982**, *680*, 331.
(17) Mouesca, J. M.; Chen, J.-L.; Noodleman, L.; Bashford, D.; Case, D. A. *J. Am. Chem. Soc.* **1994**, *116*, 11898.
(18) Blondin, G.; Girerd, J.-J. *Chem. Rev.* **1990**, *90*, 1359.
(19) Wei, P. P.; Skulan, A. J.; Wade, H.; DeGrado, W. F.; Solomon, E. I. *J. Am. Chem. Soc.* **2005**, *127*, 16098 and references therein.
(20) Chen, P.; Solomon, E. I. *Proc. Natl. Acad. Sci. U.S.A.* **2004**, *101*, 13105.
(21) Chen, P.; Solomon, E. I. *J. Am. Chem. Soc.* **2004**, *126*, 4991.
(22) Girerd, J.-J. *J. Chem. Phys.* **1983**, *79*, 1766.
(23) Bersuker, I. B.; Borshch, S. A. *Adv. Chem. Phys.* **1992**, *81*, 703.
(24) "The National Nanotechnology Initiative Strategic Plan" available at http://www.nano.gov/NNI_Strategic_Plan_2004.pdf.
(25) Evangelio, E.; Ruiz-Molina, D. *Eur. J. Inorg. Chem.* **2005**, 2957 and references therein.
(26) Dei, A.; Gatteschi, D.; Sangregorio, C.; Sorace, L. *Acc. Chem. Res.* **2004**, *37*, 827.
(27) Pierpont, C. G. *Coord. Chem. Rev.* **2001**, *99*, 216−217.
(28) Pierpont, C. G. *Coord. Chem. Rev.* **2001**, *415*, 219−221.
(29) Reingold, J. A.; Son, S. U.; Kim, S. B.; Dullaghan, C. A.; Oh, M.; Frake, P. C.; Carpenter, G. B.; Sweigart, D. A. *Dalton Trans.* **2006**, *20*, 2385 and references therein.
(30) Lever, A. B. P.; Gorelsky, S. I. *Struct. Bond.* **2004**, *107*, 77.
(31) Pierpont, C. G.; Attia, A. S. *Collect. Czech. Chem. Commun.* **2001**, *66*, 33.
(32) Pierpont, C. G.; Lange, C. W. *Prog. Inorg. Chem.* **1994**, *41*, 331.
(33) Shultz, D. A. *Comments Inorg. Chem.* **2002**, *23*, 1.
(34) Ohtsu, H.; Tanaka, K. *Angew. Chem., Int. Ed.* **2004**, *43*, 6301.
(35) Bin-Salamon, S.; Brewer, S.; Franzen, S.; Feldheim, D. L.; Lappi, S.; Shultz, D. A. *J. Am. Chem. Soc.* **2005**, *127*, 5328.
(36) (a) Ye, S. F.; Sarkar, B.; Lissner, F.; Schleid, T.; van Slageren, J.; Fiedler, J.; Kaim, W. *Angew. Chem., Int. Ed.* **2005**, *44*, 2103. (b) Chang, H.-C.; Kitagawa, S. *Angew. Chem., Int. Ed.* **2002**, *41*, 130.
(37) Benelli, C.; Dei, A.; Gatteschi, D.; Pardi, L. *Inorg. Chem.* **1989**, *28*, 1476.
(38) Bencini, A.; Carbonera, C.; Dei, A.; Vaz, M. G. F. *Dalton Trans.* **2003**, 1701.
(39) Dei, A.; Gatteschi, D.; Pardi, L. *Inorg. Chim. Acta* **1991**, *189*, 125.
(40) Caneschi, A.; Dei, A.; Lee, H.; Shultz, D. A.; Sorace, L. *Inorg. Chem.* **2001**, *40*, 408.
(41) Suenaga, Y.; Pierpont, C. G. *Inorg. Chem.* **2005**, *44*, 6183.
(42) Tao, J.; Maruyama, H.; Sato, O. *J. Am. Chem. Soc.* **2006**, *128*, 1790.
(43) Carbonera, C.; Dei, A.; Létard, J.-F.; Sangregorio, C.; Sorace, L. *Angew. Chem., Int. Ed.* **2004**, *43*, 3136.
(44) Gupta, P.; Das, A.; Basuli, F.; Castineiras, A.; Sheldrick, W. S.; Mayer-Figge, H.; Bhattacharya, S. *Inorg. Chem.* **2005**, *44*, 2081.
(45) Dei, A.; Sorace, L. *Dalton Trans.* **2003**, 3382.
(46) Calvo, M. A.; Lanfredi, A. M. M.; Oro, L. A.; Pinillos, M. T.; Tejel, C.; Tiripicchio, A.; Ugozzoli, F. *Inorg. Chem.* **1993**, *32*, 1147.
(47) Cotton, F. A.; Murillo, C. A.; Villagrán, D.; Yu, R. *J. Am. Chem. Soc.* **2006**, *128*, 3281.
(48) Bencini, A.; Daul, C. A.; Dei, A.; Mariotti, F.; Lee, H.; Shultz, D. A.; Sorace, L. *Inorg. Chem.* **2001**, *40*, 1582.
(49) Kitagawa, S.; Kawata, S. *Coord. Chem. Rev.* **2002**, *224*, 11 and references therein.
(50) Ward, M. D. *Inorg. Chem.* **1996**, *35*, 1712.
(51) Heinze, K.; Huttner, G.; Zsolnai, L.; Jacobi, A.; Schober, P. *Chem. Eur. J.* **1997**, *3*, 732.
(52) Tinti, F.; Verdaguer, M.; Kahn, O.; Savariault, J.-M. *Inorg. Chem.* **1987**, *26*, 2380.
(53) Pierpont, C. G.; Francesconi, L. C.; Hendrickson, D. N. *Inorg. Chem.* **1977**, *16*, 2367.
(54) Lloret, F.; Julve, M.; Faus, J.; Solans, X.; Journaux, Y.; Morgenstern-Badarau, I. *Inorg. Chem.* **1990**, *29*, 2232.
(55) Li, Y. T.; Yan, C. W.; Chen, Y.; Zeng, X. C.; Liao, D. Z. *Chin. J. Chem.* **2000**, *18*, 555.
(56) Dei, A.; Gatteschi, D.; Pardi, L.; Russo, U. *Inorg. Chem.* **1991**, *30*, 2589.

Scheme 1

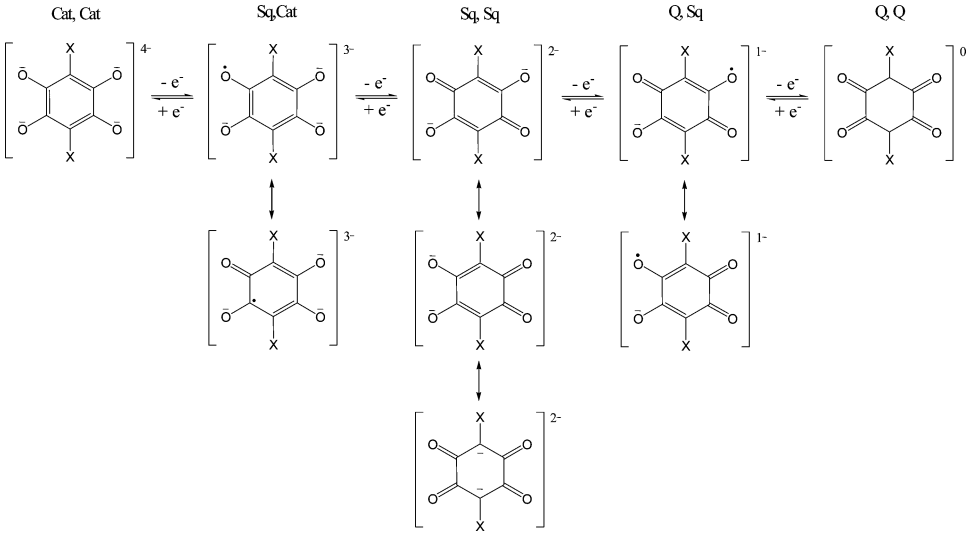

group has very recently expanded upon this work.[57b,c] Finally, the cobalt−tetraoxolene complex $[(CoTPA)_2(DHBQ)](PF_6)_3$ (where TPA is tris(2-pyridylmethyl)amine) has been reported by the Sato group.[42] This compound is formally written as (Co^{III}−(sq,cat)−Co^{III}) but exhibits both thermal and photo-induced valence tautomerism, a clear indication of the delicate balance which can exist among various charge distributions in this class of compounds.

One of the major goals of our research is to understand the correlation between the physical/photophysical properties of molecules and the spin exchange interactions that help to define their electronic structures. This requires us to be able to differentiate physical properties endemic to the isolated components of spin-coupled assemblies from those that arise due to interactions among them. One way to achieve this is to selectively incorporate (relatively) redox-inert metal ions into these systems. This allows for the oxidation states of the redox-active ligand(s) to be well defined and should lead to unambiguous characterizations of the origins of various physical phenomena. Both Cr^{III} and Ga^{III} ions are good candidates in this regard. As we have discussed previously,[58] Cr^{III} is a convenient choice as a spectroscopic probe due to its well-studied properties in the absence of spin exchange. Incorporation of Ga^{III} into a binuclear motif provides us with a spectroscopically silent d^{10} ion having a nearly identical charge-to-radius ratio to that of Cr^{III}. This synthetic design gives us an interesting platform with which to study the influence of spin exchange on the physicochemical properties of a closely related set of molecules, in which the exchange interaction can be turned "on" (i.e., $CA^{sq,cat}$ and/or Cr^{III}) or "off" (i.e., $CA^{cat,cat}$ and/or Ga^{III}). Herein, we report the synthesis, characterization, physical, and spectroscopic properties of six chloranilate bridged bimetallic complexes based on this idea (Chart 1): $[Ga_2(tren)_2(CA^{cat,cat})](BPh_4)_2$ (**1**), $[Ga_2(tren)_2(CA^{sq,cat})](BPh_4)_2(BF_4)$ (**2**), $[GaCr(tren)_2(CA^{cat,cat})](BPh_4)_2$ (**3**), $[GaCr(tren)_2(CA^{sq,cat})](BPh_4)_2(BF_4)$ (**4**), $[Cr_2(tren)_2(CA^{cat,cat})](BPh_4)_2$ (**5**), and $[Cr_2(tren)_2(CA^{sq,cat})](BPh_4)_2(BF_4)$ (**6**).

Chart 1

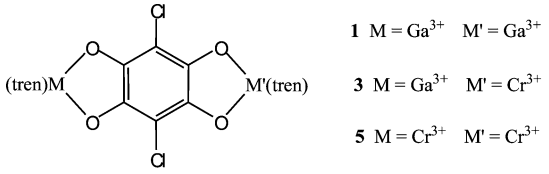

1 M = Ga^{3+} M' = Ga^{3+}

3 M = Ga^{3+} M' = Cr^{3+}

5 M = Cr^{3+} M' = Cr^{3+}

$[MM'(tren)_2(CA^{cat,cat})]^{2+}$

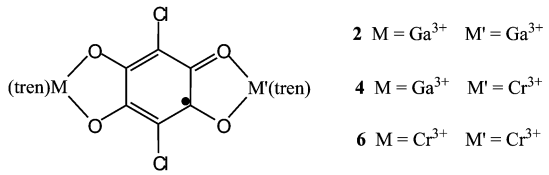

2 M = Ga^{3+} M' = Ga^{3+}

4 M = Ga^{3+} M' = Cr^{3+}

6 M = Cr^{3+} M' = Cr^{3+}

$[MM'(tren)_2(CA^{sq,cat})]^{3+}$

Experimental Section

General. All reagents and materials were used as received unless otherwise noted. Solvents were purchased from either Aldrich Chemical Co. or Fisher Scientific and distilled and degassed by the freeze−pump−thaw method. The ligand tris(2-aminoethyl)-amine (tren) was purchased from Aldrich and vacuum-distilled prior to use. $[Cr(tren)Cl_2]Cl$ was synthesized following a previously reported method.[59] All synthetic procedures involving Cr^{II} and hydrochloranilic acid (H_4CA) were performed under an inert atmosphere ($[O_2] < 1$ ppm). $[FeCp^*_2](BF_4)$ was prepared according to literature methods.[60] Elemental analyses and IR spectra were obtained through the analytical facilities at Michigan State University. ESI-MS (electrospray mass spectra) were obtained through the mass spectrometry facility at University of South Carolina using acetonitrile as the solvent.

(57) (a) Min, K. S.; Rheingold, A. L.; DiPasquale, A.; Miller, J. S. *Inorg. Chem.* **2006**, *45*, 6135. (b) Min, K. S.; DiPasquale, A.; Rheingold, A. L.; Miller, J. S. *Inorg. Chem.* **2007**, *46*, 1048. (c) Min, K. S.; DiPasquale, A. G.; Golen, J. A.; Rheingold, A. L.; Miller, J. S. *J. Am. Chem. Soc.* **2007**, *129*, 2360.

(58) Wheeler, D. E.; McCusker, J. K. *Inorg. Chem.* **1998**, *37*, 2296.

(59) Zipp, S. G.; Madan, S. K. *Inorg. Chem.* **1976**, *15*, 587.

(60) Miller, J. S.; Calabrese, J. C.; Rommelmann, H.; Chittipeddi, S. R.; Zhang, J. H.; Reiff, W. M.; Epstein, A. J. *J. Am. Chem. Soc.* **1987**, *109*, 769.

H_4CA. This compound was prepared by a modification of a previously reported method.[61] A flask was charged with H_2CA (3.0 mmol, 0.63 g) and 36% HCl (110 mmol, 9.3 g). After addition of Sn metal (3.6 mmol, 0.43 g), the mixture was refluxed under N_2 for 1 h and became a colorless solution. The hot solution was filtered under N_2 and cooled, resulting in precipitation of a white solid. The product was washed with cool degassed water and dried under vaccum overnight. The sample was stored under N_2. Yield: 0.41 g (65%). Anal. Calcd $C_6H_4O_4Cl_2$: C, 34.2; H, 1.9. Found: C, 34.2; H, 1.8.

Ga(tren)$(NO_3)_3$. A 50 mL ethanol solution of $Ga(NO_3)_3$ (15 mmol, 3.8 g) was added dropwise into a stirring solution of tren (16.5 mmol, 2.52 g) in 20 mL of ethanol resulting in the formation of a white precipitate. The solid was filtered and washed with ethanol (3 × 20 mL) and ether (20 mL) and dried under vaccum. Yield: 5.37 g (89%). Anal. Calcd $C_6H_{18}N_7O_9Ga$: C, 17.9; H, 4.5; N, 24.4. Found: C, 18.2; H, 4.6; N, 24.2.

$[Ga_2(tren)_2(CA^{cat,cat})](BPh_4)_2$ (1). Under N_2, H_4CA (0.10 mmol, 0.021 g) and Et_3N (0.40 mmol, 0.041 g) were dissolved in 3 mL of degassed MeOH. This solution was added dropwise into a solution of Ga(tren)$(NO_3)_3$ (0.20 mmol, 0.081 g) in 50 mL of MeOH. Following filtration of a green precipitate, excess $NaBPh_4$ (0.50 mmol, 0.17 g) in 10 mL MeOH solution was added to the filtrate. After standing for 30 min, white needle-shaped microcrystals were obtained. The solid was washed with MeOH (3 × 5 mL) and dried under vaccum. Yield: 0.094 g (70%). Anal. Calcd $C_{66}H_{76}N_8B_2Cl_2Ga_2O_4 \cdot 2CH_3OH$: C, 60.9; H, 6.3; N, 8.4. Found: C, 60.5; H, 6.4; N, 8.2. Crystals suitable for X-ray diffraction were obtained by carefully layering a solution of $NaBPh_4$ in methanol over the filtrate from the reaction and keeping it in the dark (under N_2) for 1 week.

$[Ga_2(tren)_2(CA^{sq,cat})](BPh_4)_2(BF_4)$ (2). Under N_2, $[Ga_2(tren)_2(CA^{cat,cat})](BPh_4)_2$ (0.50 mmol, 0.68 g) and $[FeCp^*_2](BF_4)$ (0.51 mmol, 0.21 g) were dissolved in 90 mL of acetonitrile and stirred for 30 min, resulting in a yellow-green solution. After filtration, 200 mL of ether was added to the filtrate yielding a yellow solid. The product was filtered and washed with ether (3 × 20 mL) and dried. Yield: 0.28 g (41%). Anal. Calcd $C_{66}H_{76}N_8B_3F_4Cl_2Ga_2O_4$: C, 58.1; H, 5.6; N, 8.2. Found: C, 58.5; H, 5.8; N, 8.5. IR (KBr, cm^{-1}): 3433 s, 3244 m, 2983 w, 1693 w, 1579 w, 1437 vs, 1032 s, 858 w, 738 m, 710 m, 611 w. MS [ESI, *m*/*z* (rel int)]: 240 (20) $[Ga_2(tren)_2(CA^{sq,cat})]^{3+} \cdot 2CH_3CN$, 254 (60) $[Ga_2(tren)_2(CA^{sq,cat})]^{3+} \cdot 3CH_3CN$, 267 (100) $[Ga_2(tren)_2(CA^{sq,cat})]^{3+} \cdot 4CH_3CN$, 423 (60) $[Ga(tren)(CA^{sq,sq})]^+$, 464 (20) $[Ga(tren)(CA^{sq,sq})]^+ \cdot CH_3CN$, 479 (2) $[Ga_2(tren)_2(CA^{sq,cat})(BPh_4)]^{2+}$, 1277 (2) $[Ga_2(tren)_2(CA^{sq,cat})(BPh_4)_2]^+$.

$[GaCr(tren)_2(CA^{cat,cat})](BPh_4)_2$ (3). Under N_2, H_4CA (0.13 mmol, 0.026 g) and Cr(tren)Cl_3 (0.13 mmol, 0.038 g) were combined in 50 mL of MeOH. Upon addition of Et_3N (0.25 mmol, 0.025 g), the mixture became a clear green-purple solution. After stirring 30 min, Ga(tren)$(NO_3)_3$ (0.13 mmol, 0.050 g) and Et_3N (0.25 mmol, 0.025 g) was added to the solution. When the mixture became a clear brown-green solution, excess $NaBPh_4$ (0.50 mmol, 0.17 g) in 20 mL of MeOH was added. Upon standing for 30 min, green-brown micorcrystals were obtained. The solid was washed with MeOH (3 × 10 mL) and dried under vaccum. Yield: 0.050 g (31%). Anal. Calcd $C_{66}H_{76}N_8B_2Cl_2CrGaO_4 \cdot 3CH_3OH$: C, 61.1; H, 6.5; N, 8.3. Found: C, 61.3; H, 6.5; N, 8.3. MS [ESI, *m*/*z* (rel int)]: 248 (50) $[GaCr(tren)_2(CA^{sq,cat})]^{3+} \cdot 3CH_3CN$, 262 (100) $[GaCr(tren)_2(CA^{sq,cat})]^{3+} \cdot 4CH_3CN$, 470 (4) $[GaCr(tren)_2(CA^{sq,cat})(BPh_4)]^{2+}$. Crystals suitable for X-ray diffraction were obtained by carefully layering a solution of $NaBPh_4$ in methanol over the filtrate from the reaction and keeping it in the dark (under N_2) for 1 week.

$[GaCr(tren)_2(CA^{sq,cat})](BPh_4)_2(BF_4)$ (4). The synthesis of this compound was similar to that for $[Ga_2(tren)_2(CA^{sq,cat})](BPh_4)_2(BF_4)$, except that $[GaCr(tren)_2(CA^{cat,cat})](BPh_4)_2$ (0.11 mmol, 0.15 g) was used instead of $[Ga_2(tren)_2(CA^{cat,cat})](BPh_4)_2$. The product was obtained in 73% yield (0.11 g). Anal. Calcd $C_{66}H_{76}N_8B_3Cl_2F_4CrGaO_4 \cdot CH_3CN \cdot CH_3OH$: C, 58.4; H, 5.9; N, 8.9. Found: C, 58.2; H, 5.6; N, 8.8. IR (KBr, cm^{-1}): 3443 s, 3237 s, 3055 m, 1578 m, 1437 vs, 1041 s, 857 w, 739 m, 710 m, 612 w. MS [ESI, *m*/*z* (rel int)]: 248 (70) $[GaCr(tren)_2(CA^{sq,cat})]^{3+} \cdot 3CH_3CN$, 262 (100) $[GaCr(tren)_2(CA^{sq,cat})]^{3+} \cdot 4CH_3CN$, 470 (4) $[GaCr(tren)_2(CA^{sq,cat})(BPh_4)]^{2+}$.

$[Cr_2(tren)_2(CA^{cat,cat})](BPh_4)_2$ (5). In a drybox, a solution of $CrCl_2$ (0.20 mmol, 0.025 g) in 10 mL of MeOH was added dropwise to a rapidly stirring solution of tren (0.22 mmol, 0.035 g) in 10 mL of MeOH, resulting in a sky-blue solution. A solution of $(Et_3NH)_2$CA (0.05 mmol, 0.02 g) in 20 mL of MeOH was then added to the above solution, yielding a dark-green solution, which was stirred for additional 30 min. After addition of excess $NaBPh_4$ (0.50 mmol, 0.17 g) in 20 mL of MeOH, the solution was allowed to stand overnight, resulting in the formation of a green microcrystalline precipitate. The product was washed with MeOH (3 × 10 mL) and dried under vaccum. Yield: 0.041 g (61%). Anal. Calcd $C_{66}H_{76}N_8B_2Cl_2Cr_2O_4 \cdot 2CH_3OH$: C, 62.6; H, 6.5; N, 8.6. Found: C, 62.6; H, 6.6; N, 8.7. Crystals suitable for X-ray diffraction were obtained by carefully layering a solution of $NaBPh_4$ in methanol over the filtrate from the reaction and keeping it in the dark (under N_2) for 1 week.

$[Cr_2(tren)_2(CA^{sq,cat})](BPh_4)_2(BF_4)$ (6). The synthesis of this compound was similar to that for $[Ga_2(tren)_2(CA^{sq,cat})](BPh_4)_2(BF_4)$, except that $[Cr_2(tren)_2(CA^{cat,cat})](BPh_4)_2$ (0.20 mmol, 0.26 g) was used instead of $[Ga_2(tren)_2(CA^{cat,cat})](BPh_4)_2$. The product was obtained in 46% yield (0.13 g). Anal. Calcd $C_{66}H_{76}N_8B_3Cl_2F_4Cr_2O_4 \cdot CH_3CN \cdot 2CH_3OH$: C, 58.6; H, 6.1; N, 8.8. Found: C, 58.3; H, 5.8; N, 8.8. IR (KBr, cm^{-1}): 3439 m, 3233 s, 3054 m, 1579 m, 1415 vs, 1041 s, 855 w, 739 m, 710 m, 612 w. MS [ESI, *m*/*z* (rel int)]: 228 (17) $[Cr_2(tren)_2(CA^{sq,cat})]^{3+} \cdot 2CH_3CN$, 242 (82) $[Cr_2(tren)_2(CA^{sq,cat})]^{3+} \cdot 3CH_3CN$, 255 (100) $[Cr_2(tren)_2(CA^{sq,cat})]^{3+} \cdot 4CH_3CN$, 461 (10) $[Cr_2(tren)_2(CA^{sq,cat})(BPh_4)]^{2+}$.

Physical Measurements: X-ray Structure Determinations. Single-crystal X-ray diffraction data for **1**, **3**, and **5** were acquired at the X-ray facility of Michigan State University. Diffraction data were collected on a Siemens SMART diffractometer with graphite-monochromatic Mo Kα radiation (λ = 0.71073 Å). Data were collected at −100 °C by using an Oxford Cryosystems low-temperature device. Crystallographic data are summarized in Table 1. Lattice parameters were obtained from least-squares analyses. Crystals showed no significant decay during the data collection. Data were integrated with the program SAINT.[62] The integration method employed a three-dimensional profiling algorithm, and all data were corrected for Lorentz and polarization factors, as well as for crystal decay effects. The absorption correction program SADABS[63] was employed to correct the data for absorption effects. The structures were solved by direct methods and expanded using Fourier techniques. All structure calculations were performed with the SHELXTL 6.12 software package.[64] Anisotropic thermal parameters were refined for all non-hydrogen atoms. Hydrogen

(61) (a) Graebe *Justus Liebigs Ann. Chem*. **1868**, *146*, 31. (b) Weider, P. R.; Hegedus, L. S.; Asada, H.; D'Andreq, S. V. *J. Org. Chem.* **1985**, *50*, 4276.

(62) *SAINT, ver. 6.02a*; Bruker AXS, Inc.: Madison, WI, 2000.

(63) Sheldrick, G. M. *SADABS, ver. 2.03*; Bruker AXS, Inc.: Madison, WI, 2000.

(64) Sheldrick, G. M. *SHELXTL, ver. 6.12*; Bruker AXS, Inc.: Madison, WI, 2001.

Table 1. Crystallographic Data for $[Ga_2(tren)_2(CA^{cat,cat})](BPh_4)_2$ (**1**), $[GaCr(tren)_2(CA^{cat,cat})](BPh_4)_2$ (**3**), and $[Cr_2(tren)_2(CA^{cat,cat})](BPh_4)_2$ (**5**)

	1	**3**	**5**
formula	$C_{68}H_{84}B_2Cl_2Ga_2N_8O$	$C_{68}H_{84}B_2Cl_2CrGaN_8O$	$C_{68}H_{84}B_2Cl_2Cr_2N_8O$
M_w	1341.39	1323.67	1305.95
cryst syst	monoclinic	monoclinic	monoclinic
space group	$P2(1)/n$	$P2(1)/n$	$P2(1)/n$
a/Å	13.604(2)	13.646(6)	13.636(1)
b/Å	9.622(1)	9.668(4)	9.682(1)
c/Å	25.158(3)	25.117(10)	24.999(2)
β/°	96.093(2)	96.149(7)	96.219(3)
V/Å^3	3274.5(7)	3294(2)	3280.9(5)
Z	2	2	2
T/K	173(2)	173(2)	173(2)
D_c/g cm^{-3}	1.360	1.334	1.322
$2\theta_{max}$	50.00	50.00	50.00
reflns measured	31 855	31 578	18 115
independent reflns	5756	5801	5626
observed reflns [$I > 2\sigma(I)$]	3541	3852	3157
μ(Mo Kα)/cm^{-1}	0.962	0.712	0.470
R_{int}	0.0945	0.1154	0.0988
R1[a]	0.0465	0.0426	0.0674
wR2[b]	0.0880	0.0844	0.0888
GOF	0.913	0.970	1.002

[a] $R1 = \sum||F_o| - |F_c||/\sum|F_o|$. [b] $wR2 = [\sum w(F_o^2 - F_c^2)^2/\sum w(F_o^2)^2]^{1/2}$, $w = 1/[\sigma^2(F_o^2) + (aP)^2 + bP]$, where $P = [F_o^2 + 2F_c^2]/3$.

atoms were localized in their calculated positions and refined by using the riding model. For the mixed-metal complex **3**, each metal site was randomly disordered corresponding to occupancy by either Ga^{III} or Cr^{III}. Further details concerning the structure determinations may be found in Supporting Information.

Cyclic Voltammetry. Electrochemical measurements were carried out in a N_2-filled dry box (Vacuum Atmospheres) using a BAS CV-50W electrochemical analyzer. A standard three-electrode configuration was employed consisting of Pt working and counter electrodes and a $Ag/AgNO_3$ reference electrode. Compounds were dissolved in CH_3CN that was 0.1 M in NBu_4PF_6; the CH_3CN had been distilled from both $KMnO_4$ and CaH_2, passed over a silica column, and then degassed by the freeze−pump−thaw method. Data were acquired at a scan rate of 100 mV s^{-1}. Ferrocene was added to all solutions to provide for internal calibration.

Electronic Absorption Measurements. Electronic absorption spectra were recorded using a Hewlett-Packard 8452A diode-array spectrophotometer for complexes **1**, **3**, and **5**. The high-resolution spectra of complexes **2**, **4**, and **6** were obtained on a U-4001 UV−vis−NIR spectrophotometer at a spectral resolution of 0.20 nm. Data were obtained on samples dissolved in CH_3CN that had been passed over a silica column, doubly distilled (from $KMnO_4$, then CaH_2), degassed, and stored under an inert atmosphere. All solutions were prepared under an inert atmosphere in 1 cm pathlength sealed optical cells.

Variable-Temperature Magnetic Susceptibility. Magnetic susceptibility data were collected using a Quantum Design MPMS SQUID magnetometer interfaced to an IBM PC. Data were collected in an applied field of 1 T. Following each temperature change, the system was kept at the new temperature for an additional 5 min before data collection to ensure thermal equilibration of the sample. Data were corrected for diamagnetism of the sample using Pascal's constants, as well as the measured susceptibility of the sample holder and reported herein as effective magnetic moments. Magnetic data for complex **5** were fit to an operator-equivalent form of the spin Hamiltonian given in eq 2 using MAGFIT.[65]

Low-Temperature Steady-State Emission Measurements. All samples were prepared under an inert atmosphere by dissolution in a mixture of butyronitrile and propionitrile (9:2), both of which had been distilled from CaH_2, degassed, and stored nder an inert atmosphere. Emission spectra were acquired at 90 K using an Instruments SA/Jobin Yvon-Spex Fluoromax photon-counting fluorimeter equipped with a Xe arc lamp excitation source and a Hamamatsu R928P photomultiplier tube operating at −900 V dc. Temperature control was achieved using heating filaments and two matched diodes placed approximately equidistant above and below the sample region of a Janis SVT-100 optical cryostat. The heaters and the diodes were coupled to two LakeShore model 321 automated temperature control units. Data were obtained on thoroughly deoxygenated solutions of each compound having an optical density of ca. 0.2 at the excitation wavelength. Background measurements on the solvent blanks revealed no signals other than the expected Raman lines of the neat solvent.

Resonance Raman Spectroscopy. Resonance Raman spectra were acquired using both the 457.9 (50mW) and 488.1 nm (30mW) outputs of an Ar-ion laser (Coherent model Innova 70), as well as the 647.4 nm line (250 mW) from a Kr-ion laser (Coherent model Innova 90). The samples were thoroughly degassed and placed in a sealed spinning cell. Scattered light was collected using an $F = 0.7$ spheric lens at a 90° geometry. Spectra were recorded using a Triax 550 spectrophotometer equipped with Spectrum One liquid-nitrogen-cooled CCD using 1800 ln mm^{-1} grating (Horiba/Jobin Yvon). The Raleigh line was rejected using a holographic notch filter (Kaiser Optical Systems); the spectral slit width used for data acquisition was 4 cm^{-1}. A total of 10−20 10-s spectra were averaged for each sample.

DFT Calculations. An electronic structure calculation of the $CA^{sq,cat}$ ligand was carried out using density functional theory as implemented in Gaussian 98.[66] The B3PW91 functional was used in the calculation which contains the three-parameter exchange of Becke (B3)[67] and Perdew and Wang's 1991 gradient-corrected correlation functional (PW91).[68−72] The calculation was performed using tight convergence criteria.[73] Analysis of the atomic charges and spin densities were performed using the natural population

(65) Schmitt, E. Ph.D. Dissertation. Department of Chemistry, University of Illinois, Urbana−Champaign, IL, 1996.

Scheme 2

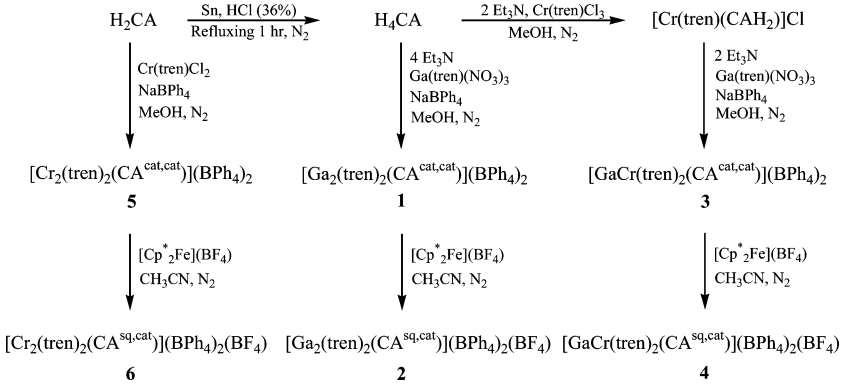

analysis (NPA) framework developed by Weinhold et al.[74] The initial geometry of the molecule was generated using GaussView[75] and subsequently optimized using the UB3PW91 functional and a 6-311G** basis set with imposed symmetries of C_{2v} and D_{2h}. Final geometries were subjected to frequency calculations at the UB3PW91/6-311G** level; the absence of any imaginary frequencies indicated that the final structures corresponded to global minima. Single-point calculations were performed using the unrestricted density functional UB3PW91 with the 6-311G** basis set assuming a doublet ground state and a molecular charge of 3−.

Results and Discussion

Synthesis and Characterization. By combining the reversible redox properties of quinoidal ligands with relatively redox-inert metal ions, we sought to develop a series of complexes that would enable us to systematically study the effect of spin exchange on the physical and photophysical properties of molecules. In particular, we wanted to be able to clearly differentiate physical properties endemic to the components of these assemblies from those arising due to interactions among those components. Complexes prepared for this study are shown in Chart 1; the synthetic routes are summarized in Scheme 2. As discussed in our previous study,[58] tren represents a convenient choice as a counterligand due to the fact that it forms a single isomer when bound to a metal, and furthermore will not contribute directly to the absorption spectra of the compounds.

The dianionic form of chloranilic acid is very stable in air in the solid state, as well as in solution under both basic and acidic conditions. It is therefore reasonable that most compounds containing chloranilate have been prepared from CA^{2-} starting materials, and consequently, the CA tended to be in the (sq,sq) form in these compounds. Upon one-electron reduction, CA^{2-} is converted into its radical form $[CA^{sq,cat}]^{3-}$. To the best of our knowledge, neither the protonated or deprotonated form of $CA^{sq,cat}$ has been isolated as a free ligand. The only report claiming detection of $CA^{sq,cat}$ indicated its formation in aqueous NaOH in the presence of $Na_2S_2O_4$.[76] Due in part to the very negative reduction potential required to fully reduce the ligand to its (cat,cat) form (i.e., $[CA^{cat,cat}]^{4-}$), all efforts to prepare the $CA^{cat,cat}$ ligand in basic or neutral conditions failed. However, under strongly acidic conditions H_4CA can be readily prepared by reducing H_2CA in the presence of indium(I), germanium(II), or tin(0).[61,77,78] Provided the solid is rigorously dried, it can be stored in air; however, storing under N_2 is recommended.

Our choice of metals was motivated in part by a desire to limit redox activity to the chloranilate bridge. In addition, the well-documented physical and photophysical properties of Cr^{III} will simplify the identification of features tied to the presence of spin exchange across this series of compounds. A thorough search of the literature yielded only one well-studied example of this structural motif for chromium(III). The synthesis of $[Cr_2(CTH)_2(DHBQ)](PF_6)_3$ by Dei and coworkers[56] was based on redox processes presumably occurring among two Cr^{II} ions and 2,5-dihydroxy-1,4-benzoquinone in the presence of base. Exposure of the solution to air resulted in the formation of the dichromium(III) complex in which the bridge is in the 3− oxidation state. Our synthetic route follows this same initial approach, i.e., a redox reaction between a Cr^{II} starting material, $Cr(tren)Cl_2$, and the CA ligand in the (sq,sq) form. This leads to the formation of a (Cr^{III}−(cat,cat)−Cr^{III}) complex, namely $[Cr_2(tren)_2(CA^{cat,cat})]^{2+}$,

(66) Frisch, M. J.; Trucks, G. W.; Schlegel, H. B.; Scuseria, G. E.; Robb, M. A.; Cheeseman, J. R.; Zakrzewski, V. G.; Montgomery, J. A., Jr.; Stratmann, R. E.; Burant, J. C.; Dapprich, S.; Millam, J. M.; Daniels, A. D.; Kudin, K. N.; Strain, M. C.; Farkas, O.; Tomasi, J.; Barone, V.; Cossi, M.; Cammi, R.; Mennucci, B.; Pomelli, C.; Adamo, C.; Clifford, S.; Ochterski, J.; Petersson, G. A.; Ayala, P. Y.; Cui, Q.; Morokuma, K.; Malick, D. K.; Rabuck, A. D.; Raghavachari, K.; Foresman, J. B.; Cioslowski, J.; Ortiz, J. V.; Stefanov, B. B.; Liu, G.; Liashenko, A.; Piskorz, P.; Komaromi, I.; Gomperts, R.; Martin, R. L.; Fox, D. J.; Keith, T.; Al-Laham, M. A.; Peng, C. Y.; Nanayakkara, A.; Gonzalez, C.; Challacombe, M.; Gill, P. M. W.; Johnson, B. G.; Chen, W.; Wong, M. W.; Andres, J. L.; Head-Gordon, M.; Replogle, E. S.; Pople, J. A. *Gaussian 98*, revision A.4; Gaussian, Inc.: Pittsburgh, PA, 1998.

(67) Becke, A. D. *J. Chem. Phys.* **1993**, *98*, 5648.

(68) Burke, K.; Perdew, J. P.; Wang, Y. In *Electronic Density Functional Theory: Recent Progress and New Directions*; Dobson, J. F., Vignale, G., Das, M. P., Eds.; Plenum: New York, 1998.

(69) Perdew, J. P. In *Electronic Structure of Solids'91*; Ziesche, P., Eschrig, H., Eds.; Akademie Verlag: Berlin, 1991.

(70) Perdew, J. P.; Chevary, J. A.; Vosko, S. H.; Jackson, K. A.; Pederson, M. R.; Singh, D. J.; Fiolhais, C. *Phys. Rev. B* **1992**, *46*, 6671.

(71) Perdew, J. P.; Chevary, J. A.; Vosko, S. H.; Jackson, K. A.; Pederson, M. R.; Singh, D. J.; Fiolhais, C. *Phys. Rev. B* **1993**, *48*, 4978.

(72) Perdew, J. P.; Burke, K.; Wang, Y. *Phys. Rev. B* **1996**, *54*, 16533.

(73) Frisch, M. J.; Frisch, A. *Gaussian 98 User's Reference*; Gaussian, Inc.: Pittsburgh, PA, 1998.

(74) Glendening, E. D.; Reed, A. E.; Carpenter, J. E.; Weinhold, F. *NBO 3.1*; Theoretical Chemistry Institute, University of Wisconsin: Madison, WI, 1994.

(75) *GaussView* 2.1; Gaussian, Inc.: Pittsburgh, PA, 2000.

(76) Broze, M.; Luz, Z. *J. Phys. Chem.* **1967**, *71*, 3690.

(77) Swavey, S.; Gould, E. S. *Inorg. Chem.* **2000**, *39*, 1200.

(78) Babich, O. A.; Gould, E. S. *Inorg. Chem.* **2000**, *39*, 4119.

which we were able to isolate by direct precipitation from the solution prior to oxidation by air or other chemical oxidants.

The ability to selectively incorporate spectroscopically silent metal ions into the bridged dimer motif was deemed desirable to aid in the interpretation of the photophysical properties of these compounds. Ga^{III} was an obvious choice in this regard given its d^{10} electronic configuration and nearly identical charge-to-radius ratio as compared to Cr^{III}. Ga^{III} complexes of semiquinone ligands have been prepared by several groups,[79−84] but no tetraoxolene-based complexes have been reported. In contrast to the redox-based approach used for the Cr^{III} complexes (as well as for the preparation of $Ga(SQ)_3$ systems from Ga metal[80−82]), we were able to directly prepare $[Ga_2(tren)_2(CA^{cat,cat})](BPh_4)_2$ in high yield by using the $CA^{cat,cat}$ form of the ligand and a Ga^{III} precursor as starting materials.

Synthesis of the GaCr mixed-metal dimeric complex proved to be the most challenging. The key step is the formation of a $Cr^{III}-CA^{cat,cat}$ monomer complex, which formed by reacting the tren-capped Cr^{3+} precursor with the doubly deprotonated $CA^{cat,cat}$ ligand, $(H_2CA)^{2-}$. Unfortunately, the $Cr^{III}-CA^{cat,cat}$ monomer complex could not be cleanly isolated: the compound is stable in solution for ca. 1 h but then slowly forms an insoluble precipitate even under oxygen-free conditions. However, addition of base to a solution of the monomer prior to decomposition yields the fully deprotonated $[Cr(tren)(CA^{cat,cat})]^{2-}$ species which can then bind the $[Ga^{III}(tren)]^{3+}$ fragment, resulting in the formation of the $[CrGa(tren)_2(CA^{cat,cat})]^{2+}$ mixed-metal complex.

Handling and storage of all of the $CA^{cat,cat}$-containing complexes must be carried out in a strictly inert atmosphere due to the facile oxidation of these compounds to their $CA^{sq,cat}$ and/or $CA^{sq,sq}$ forms. This oxidation occurs easily when even a trace amount of oxygen is present. Following this consideration, however, solid complexes of formula $[M-(CA^{sq,cat})-M']$ could be prepared from the $CA^{cat,cat}$ complexes by controlled oxidation using $[FeCp^*_2](BF_4)$ in acetonitrile and then precipitated as powders by addition of diethyl ether. The $[M-CA^{sq,cat}-M']^{3+}$ complexes are much more stable than their $CA^{cat,cat}$ analogues in both solid state and in solution. Nevertheless, these compounds were also handled under air-free conditions during the preparation of samples for physical and photophysical measurements.

In principle, further oxidation of the $CA^{sq,cat}$-containing complex by stronger oxidants or direct reaction of the metal-ion precursors with the $CA^{sq,sq}$ ligand could lead to the formation of $CA^{sq,sq}$-bridged dimers. Unfortunately, all of our attempts at the isolation of these molecules have failed. It should be noted that other $CA^{sq,sq}$-containing binuclear chromium(III) complexes of the form $[Cr_2(CA^{sq,sq})(L)_4](ClO_4)_4$ have been reported from the reaction of chloranilic acid with $Cr(ClO_4)_3$ and a number of other capping ligands (e.g., L = Me-phen, Me_2-phen, Cl-phen, en, pn).[55] Efforts to modify our system to allow us access to these $CA^{sq,sq}$-bridged complexes are continuing.

Elemental analyses and ESI-MS data of complexes **1**−**6** are consistent with the formation of the corresponding homo- and heterobimetallic dimers. For example, complex **2** in acetonitrile solution shows three main cation peaks corresponding to $[Ga_2(tren)_2(CA^{sq,cat})]^{3+}\cdot 2CH_3CN$ (m/z = 240), $[Ga_2(tren)_2(CA^{sq,cat})]^{3+}\cdot 3CH_3CN$ (m/z = 254), and $[Ga_2(tren)_2(CA^{sq,cat})]^{3+}\cdot 4CH_3CN$ (m/z = 267), respectively, consistent with the formation of $[Ga_2(tren)_2(CA^{sq,cat})]^{3+}$ dimer; the ESI-MS data also provide an indication that the dimer species are stable in solution. It is particularly notable that the ESI-MS spectra of the mixed-metal complexes **3** and **4** each exhibited a single molecular ion peak with isotope patterns consistent with a $Cr^{III}Ga^{III}$ composition; no signals corresponding to either of the homobimetallic analogues (i.e., $Ga^{III}Ga^{III}$ or $Cr^{III}Cr^{III}$) were detected. This result along with magnetic data to be discussed later clearly establishes that complexes **3** and **4** are indeed heterobimetallic species as opposed to a mixture of $Ga^{III}Ga^{III}$ and $Cr^{III}Cr^{III}$ dimers.

Single-Crystal X-ray Structures. Single-crystal X-ray structure determinations were carried out for complexes **1**, **3**, and **5**. The structural features of the bridging tetraoxolene ligand in dimers of this sort have been reported in three of its possible oxidation states, namely the (sq,sq), (sq,cat), and (cat,cat) forms.[49] Among these structures, the dianionic (sq,sq) quinoid formulations appear more frequently than either of their reduced (sq,cat) and (cat,cat) forms in single-crystal X-ray structures. In general, changes in metric details within the ligand follow the trends one might expect upon reduction from a bis-semiquinone- to bis-catechol-type oxidation state. For example, in $[(CoTPA)_2(DHBQ)](PF_6)_2$ the C−O bond distances are structurally distinguishable at 1.289(3) and 1.281(3) Å with variations in C−C bond lengths within the ring of up to 0.131 Å.[42] Upon reduction to $[(CoTPA)_2(DHBQ)](PF_6)_3$, the C−O bonds lengthen to 1.324(6) and 1.326(6) Å:[42] these values combined with the much narrower spread in C−C bond distances (from 1.381(7) to 1.457(8) Å) reflects the more delocalized nature of the radical form of the ligand. Structural changes upon further reduction appear to be much less dramatic: the C−O distances (1.311(8) and 1.313(8) Å), as well as the narrow C−C distance range (1.39−1.45 Å) in the dinuclear Co^{III} complex $[Co_2(DHBQ)(tdpme)_2](BF_4)_2$ (tdpme = $CH_3C(CH_2PPh_2)_3$),[51] is not markedly different from the aforementioned compound despite its formulation as a tetraanionic (cat,cat)-type ligand.

Complexes **1**, **3** and **5** are isostructural and crystallize with two methanol solvate molecules per dimeric unit in the monoclinic space group $P2(1)/n$. Crystallographic details are

(79) Prokof'ev, A. I.; Bubnov, N. N.; Solodovnikov, S. P.; Kabachnik, M. I. *Dokl. Akad. Nauk SSSR* **1979**, *245*, 178.
(80) Lange, C. W.; Conklin, B. J.; Pierpont, C. G. *Inorg. Chem.* **1994**, *33*, 1276.
(81) Adams, D. M.; Rheingold, A. L.; Dei, A.; Hendrickson, D. N. *Angew. Chem., Int. Ed. Engl.* **1993**, *32*, 391.
(82) Ozarowski, A.; McGarvey, B. R.; El-Hadad, A.; Tian, Z.; Tuck, D. G.; Krovich, D. J.; DeFotis, G. C. *Inorg. Chem.* **1993**, *32*, 841.
(83) Brown, M. A.; El-Hadad, A. A.; McGarvey, B. R.; Sung, R. C. W.; Trikha, A. K.; Tuck, D. G. *Inorg. Chim. Acta* **2000**, *613*, 300−302.
(84) (a) Yeh, R. M.; Raymond, K. N. *Inorg. Chem.* **2006**, *45*, 1130. (b) Johnson, D. W.; Raymond, K. N. *Inorg. Chem.* **2001**, *40*, 5157. (c) Kersting, B.; Meyer, M.; Powers, R. E.; Raymond, K. N. *J. Am. Chem. Soc.* **1996**, *118*, 7221. (d) Sofen, S. R.; Ware, D. C.; Cooper, S. R.; Raymond, K. N. *Inorg. Chem.* **1979**, *18*, 234.

Table 2. Selected Bond Distances (Å) and Angles (deg) for $[Ga_2(tren)_2(CA^{cat,cat})](BPh_4)_2$ (**1**), $[GaCr(tren)_2(CA^{cat,cat})](BPh_4)_2$ (**3**), and $[Cr_2(tren)_2(CA^{cat,cat})](BPh_4)_2$ (**5**)

	1	**3**	**5**
	Bond Distances (Å)		
M(1)−O(1)[a]	1.932(2)	1.940(2)	1.944(3)
M(1)−O(2)	1.922(2)	1.923(2)	1.918(3)
M(1)−N(1)	2.064(3)	2.073(2)	2.081(3)
M(1)−N(2)	2.086(3)	2.079(2)	2.105(4)
M(1)−N(3)	2.176(3)	2.149(2)	2.082(3)
M(1)−N(4)	2.099(3)	2.086(2)	2.083(3)
O(1)−C(8)	1.375(4)	1.370(3)	1.364(4)
O(2)−C(9)	1.348(4)	1.349(3)	1.348(4)
C(7)−C(8)	1.392(5)	1.394(4)	1.401(5)
C(8)−C(9)	1.399(5)	1.405(4)	1.403(5)
C(7)−C(9A)[b]	1.402(5)	1.389(4)	1.393(5)
M···M[c]	7.61	7.64	7.67
	Bond Angles (deg)		
O(1)−M(1)−N(1)	90.67(10)	92.16(8)	93.34(11)
O(1)−M(1)−N(2)	101.46(10)	100.31(8)	95.19(13)
O(1)−M(1)−N(3)	95.07(11)	94.77(9)	99.65(12)
O(1)−M(1)−N(4)	173.25(10)	174.35(8)	175.58(13)
O(2)−M(1)−O(1)	88.10(9)	87.05(7)	86.39(11)
O(2)−M(1)−N(1)	176.61(11)	177.89(9)	178.88(14)
O(2)−M(1)−N(2)	87.72(11)	87.06(8)	86.61(12)
O(2)−M(1)−N(3)	85.81(11)	86.31(9)	86.43(12)
O(2)−M(1)−N(4)	96.67(10)	96.81(8)	96.77(12)
N(1)−M(1)−N(2)	95.62(11)	95.00(9)	92.34(14)
N(1)−M(1)−N(3)	91.15(12)	91.81(9)	94.69(13)
N(1)−M(1)−N(4)	84.30(11)	83.83(9)	83.44(12)
N(2)−M(1)−N(3)	162.03(11)	163.18(9)	163.17(13)
N(2)−M(1)−N(4)	83.56(11)	84.04(9)	81.95(14)
N(4)−M(1)−N(3)	80.57(12)	81.42(9)	83.68(14)

[a] M = Ga for **1**, M = Ga or Cr for **3** (see text for details), and M = Cr for **5**. [b] Symmetry A: $1 - x, 2 - y, -z$. [c] Nonbonding metal-to-metal distance.

given in Table 1, with selected bond distances and angles given in Table 2. In all three cases, the complexes are situated on crystallographic inversion centers, making only half of the dimer unique. The fact that this was found to be the case for the mixed-metal $[CrGa(tren)_2(CA^{cat,cat})]^{2+}$ complex indicates that the identity of the metal ion in the asymmetric unit in this compound varies randomly throught the crystalline lattice.

We take the structure of Cr^{III} dimer (complex **5**) as our basis for a detailed structure description of this series of molecules; ORTEP drawings of all three $CA^{cat,cat}$-bridged dimers are shown in Figure 1. The environments about the metal ions are distorted octahedrons with four aliphatic nitrogens from the tren capping ligand and two oxygen donors from the chloranilate bridge. Bond angles in the coordination sphere deviate slightly from the expected 90° and 180°, due mainly to the reduced bite angle of the tetradentate ligand in spanning all four coordination sites. The Cr−N bond distances are unremarkable with an average of 2.088 Å, similar to those observed for related complexes such as [Cr(tren)(3,6-DTBCat)](ClO_4) (where 3,6-DTBCat is 3,6-di-*tert*-butylorthocatechol):[85] in this latter complex, the Cr−N bond distances exhibit an average value of 2.098 Å, which is slightly longer than the corresponding average for the semiquinone analogue [Cr(tren)(3,6-DTBSQ)](ClO_4)$_2$ (2.07 Å).[58] The Cr−O distances in the $CA^{cat,cat}$-bridged dimer

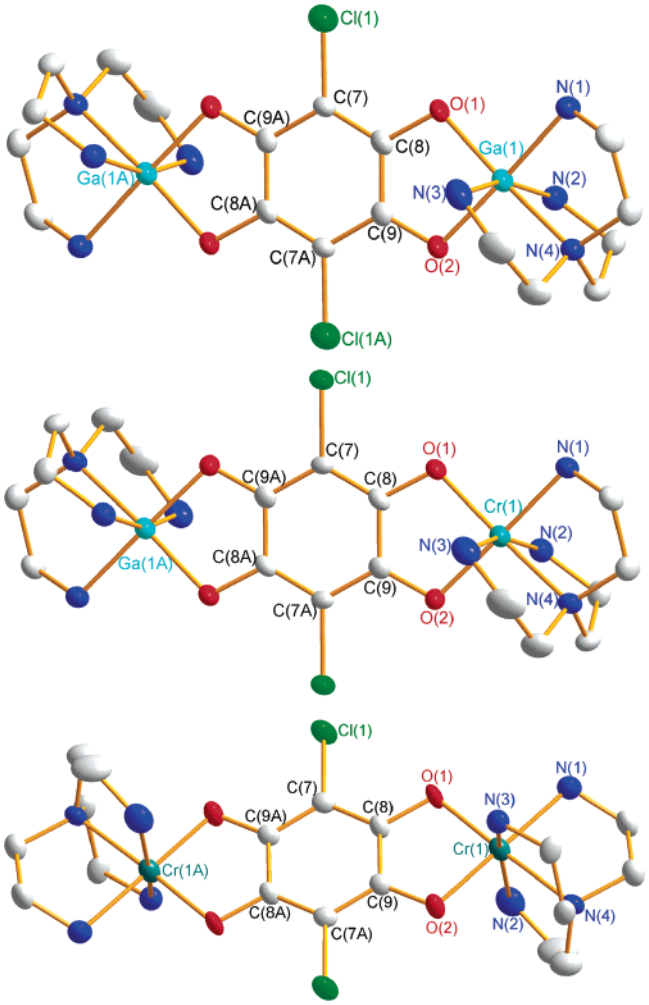

Figure 1. Drawings of the cations of $[Ga_2(tren)_2(CA^{cat,cat})](BPh_4)_2$ (**1**) (top), $[GaCr(tren)_2(CA^{cat,cat})](BPh_4)_2$ (**3**) (middle), and $[Cr_2(tren)_2(CA^{cat,cat})](BPh_4)_2$ (**5**) (bottom) obtained from single-crystal X-ray structure determinations. Atoms are represented as 50% probability thermal ellipsoids.

are in the range of 1.918−1.944 Å; the difference between two Cr−O bonds in complex **5** is little larger than what is observed for [Cr(tren)(3,6-DTBCat)](ClO_4) and smaller than that of $[Cr(tren)(3,6\text{-DTBSQ})]^{2+}$. The chloranilate bridging ligand is essentially planar with the two metal centers located 0.11 Å above and below this plane, respectively. This results in a chair-type conformation of the Cr−CA−Cr fragment with a dihedral angle between the ligand and O−Cr−O planes of 4.5°. The intradimer metal−metal distance of 7.67 Å is determined by the geometry of the bridging ligand.

It has been found that, for quinoidal ligands bound to first-row metals, the bond lengths within the ring provide a strong indication as to the oxidation state of the ligand.[31,32,86] Specifically, if the ligand exists in the catecholate form all of the C−C bond distances should be nearly identical due to the aromatic nature of the catecholate species. The semiquinone form, however, should exhibit alternating short and long C−C bonds because of the more localized nature of the double bonds within the ring. The nonaromatic nature of the semiquinone ligand in $[Cr(tren)(3,6\text{-DTBSQ})]^{2+}$ was clearly seen from the alternating single/double bond character

(85) Rodriguez, J. H.; Wheeler, D. E.; McCusker, J. K. *J. Am. Chem. Soc.* **1998**, *120*, 12051.

(86) Pierpont, C. G.; Buchanan, R. M. *Coord. Chem. Rev.* **1981**, *38*, 45.

Table 3. Electrochemical Properties of $[MM'(tren)_2(CA)]^{n+}$ (M, M′ = Ga^{III} and/or Cr^{III})[a]

	3+/2+		4+/3+		5+/4+
compounds	$E_{1/2}$ (V)	ΔE (mV)[b]	$E_{1/2}$ (V)	ΔE (mV)[b]	E_{ox} (V)[c]
$[Ga_2(tren)_2(CA^{cat,cat})]^{2+}$ (**1**)	−0.792	68	−0.052	115	> 0.4
$[CrGa(tren)_2(CA^{cat,cat})]^{2+}$ (**3**)	−0.824	71	0.049	114	> 0.4
$[Cr_2(tren)_2(CA^{cat,cat})]^{2+}$ (**5**)	−0.833	67	0.115	147	> 0.4

[a] All potentials are referenced to the ferrocenium/ferrocene couple ($E_{1/2}$ = 0.087 V). [b] $\Delta E = E_p^{anodic} - E_p^{cathodic}$. [c] Irreversible oxidation.

of the intraring C−C bonds.[58] Upon one-electron reduction to form the catecholate analogue, the C−C bond distances became more equivalent, although a longer C−C bond for the carbons bound to the ortho oxygens was noted.[85] In the current $CA^{cat,cat}$-bridged complex, the C−C bond distances within the ring encompass a relatively narrow range of 1.393−1.402 Å. This strongly supports an aromatic character for the ligand, reflecting the fully reduced nature of chloranilate in this compound. Our structural data are also consistent with that of the free catechol, 2,3,5,6-tetrahydroxy-*p*-phenylenediammonium dichloride, where all of the ring bond distances span a range from 1.386 to 1.404 Å.[87]

In addition to the ring C−C bonds, the C−O bond distances can also be used as indicators of the quinone oxidation state.[31,32,86] Generally, these two bond distances are somewhat different in semiquinone complexes, consistent with the pseudo-double-bond and single-bond character of the C−O groups, whereas this difference is statistically negligible in $[Cr(tren)(3,6\text{-DTBCat})]^+$ at 1.372 and 1.378 Å.[85] In the present $Cr^{III}-CA^{cat,cat}-Cr^{III}$ complex, though the difference of the C−O bond distances of 1.364 and 1.348 Å is larger than that observed for $[Cr(tren)(3,6\text{-DTBCat})]^+$, the bond lengths are still significantly longer than the average distance of 1.31 Å found for $[Cr(tren)(3,6\text{-DTBSQ})]^{2+}$.[58] Again, these metrics are consistent with a catechol-like formulation for the ligand in this complex.

Structural features for complexes **1** and **3** are qualitatively similar to those just described for $[Cr_2(tren)_2(CA^{cat,cat})]^{2+}$. As expected, there are some differences in the specifics, owing to the fact that coordination to Ga^{III} is similar to, but not exactly the same as, binding to Cr^{III}. The most significant variation is found in the observed M···M distances, which shortens by ∼0.07 Å in the digallium(III) complex relative to complex **5**. Some variability is also noted in a few of the bond angles associated with the coordination sphere of the metals. However, for the most part these structural differences appear to be minor. Most significant is the homogeneity in the bond distances within the chloranilate ligand, which in conjunction with the magnetic and spectroscopic data described below helps to confirm the $CA^{cat,cat}$ oxidation state of the bridge in all three complexes.

Given the preceding discussion concerning changes in various bond distances between the semiquinone and catechol oxidation states, structural comparisons among complexes **1**, **3**, and **5** ($CA^{cat,cat}$) and **2**, **4**, and **6** ($CA^{sq,cat}$) would be highly desirable. Unfortunately, extensive efforts to grow X-ray quality crystals of the latter three complexes have thus far been unsuccessful.

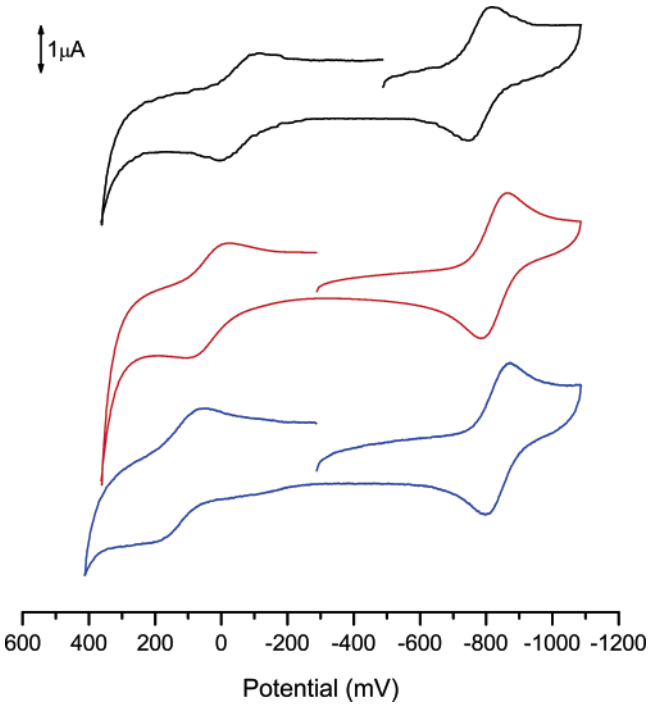

Figure 2. Cyclic voltammograms of $[Ga_2(tren)_2(CA^{cat,cat})](BPh_4)_2$ (top), $[GaCr(tren)_2(CA^{cat,cat})](BPh_4)_2$ (middle), and $[Cr_2(tren)_2(CA^{cat,cat})](BPh_4)_2$ (bottom). All data were acquired in degassed acetonitrile containing 0.1 M NBu_4PF_6 at a scan rate of 100 mV s^{-1}. See Table 3 for further details.

Electrochemistry. Metal complexes containing quinoidal ligands typically exhibit rich electrochemical behavior due to the multiple oxidation states of the ligand that can be accessed. However, when coupled with redox-active metal centers, the assignment of electrochemical waves in a cyclic voltammagram can be difficult. This situation is compounded in the case of tetraoxolene-containing assemblies, in which four ligand-based redox reactions are possible (Scheme 1). Dei and co-workers reported the electrochemistry of complexes of the form $[M_2(CTH)_2(DHBQ)]^{n+}$, where M = Cr, Mn, Fe, and Ni.[56] As expected, these workers observed multiple redox waves for all of these compounds. The feature occurring at the most negative potential ($E_{1/2}$ < −1 V vs ferrocene) was assigned as a ligand-based process on the basis of the relative invariance of its position across the four-membered series. Assignments for the features observed at more positive potentials are less definitive, although the fact that they are sensitive to the identity of the metal ion suggests that they are not ligand-localized.

Assigning features in the cyclic voltammograms of our CA-bridged complexes should be more straightforward due to the relative redox stability of the metal ions we have employed. Electrochemical data and the CV traces from which they derive are given in Table 3 and Figure 2,

(87) Akutagawa, T.; Nakamura, T. *Cryst. Growth Des.* **2006**, *6*, 70.

respectively. The data reveal that each compound undergoes one reversible one-electron redox process near −0.8 V, one quasi-reversible process in the range of 0 to +0.1 V, and the onset of an irreversible wave just past +0.4 V. The data for all three compounds are strikingly similar, suggesting that the same redox process is being sampled in the Ga^{III}-Ga^{III}, $Cr^{III}Ga^{III}$, and $Cr^{III}Cr^{III}$ complexes. This similarity coupled with the redox inertness of Ga^{III} allows us to confidently assign all of the observed features in all three complexes as tetraoxolene-based electron-transfer processes, i.e.,

$$[MM'(tren)_2(CA^{cat,cat})]^{2+} \underset{+e^-}{\overset{-e^-}{\rightleftharpoons}} [MM'(tren)_2(CA^{sq,cat})]^{3+} \quad (1a)$$

$$[MM'(tren)_2(CA^{sq,cat})]^{3+} \underset{+e^-}{\overset{-e^-}{\rightleftharpoons}} [MM'(tren)_2(CA^{sq,sq})]^{4+} \quad (1b)$$

$$[MM'(tren)_2(CA^{sq,sq})]^{4+} \xrightarrow{-e^-} [MM'(tren)_2(CA^{q,sq})]^{5+} \quad (1c)$$

The first and the second waves are thus ascribed to the (sq,cat)/(cat,cat), and (sq,sq)/(sq,cat) couples, respectively (eqs 1a and 1b), while the irreversible process observed past +400 mV is assigned as an oxidation to the (q,sq) form of the chloranilate bridge (eq 1c). The fact that the most chemically reversible process corresponds to the (cat,cat)/(sq,cat) couple is reasonable given that both of these oxidation states of the bridging ligand yield isolable dinuclear complexes. Similarly, the quasi-reversiblity of the wave corresponding to oxidation of the (sq,cat) form suggests a reason why we have had difficulty isolating complexes containing the $[CA^{sq,sq}]^{2-}$ ligand. The chelating ability of chloranilate is expected to degrade further upon oxidation to the (q,sq) form, hence the decomposition that is apparent at more positive potentials.

Reductive scans out to −2.0 V for the chromium-containing compounds failed to show any signal attributable to the Cr^{III}/Cr^{II} couple. Again, this is consistent with what has been observed in other Cr^{III}−catecholate complexes and testifies to the stability of this oxidation state of the metal when bound to the quinoidal ligand.

Electronic Structure. A. Magnetic Susceptibility. Variable-temperature magnetic susceptibility data for solid samples of complexes **2**−**6** were acquired in the range of 2−350 K: these data are plotted in Figure 3. Complex **2** is comprised of two diamagnetic Ga^{III} ions and a simple organic radical. The magnetic data for complex **2** confirm this formulation, revealing a temperature-independent magnetic moment of $\mu_{eff} = 1.64 \pm 0.04\ \mu_B$, consistent with an $S = 1/2$ ground state.[88] The other magnetically dilute member of the series is $[CrGa(tren)_2(CA^{cat,cat})](BPh_4)_2$ (complex **3**). Indeed, the effective magnetic moment for this compound is temperature-independent with a value of $\mu_{eff} = 3.44 \pm 0.09\ \mu_B$. This is somewhat below but still consistent with the spin-only value of $\mu_{eff} = 3.87\ \mu_B$ expected for the $S = 3/2$ ground state of an isolated Cr^{III} ion. A slight positive slope observed in the data with increasing temperature is likely due to second-order Zeeman interactions.

The simultaneous presence of Cr^{III} and the trianionic form of chloranilate in complexes **4**−**6** is expected to give rise to intramolecular spin exchange.[58,85,89−93] The variable-temperature magnetic data for complex **4** were found to be constant in the range of 5−350 K at a value of $\mu_{eff} = 2.72 \pm 0.05\ \mu_B$. This is characteristic of an $S = 1$ state ($\mu_{eff}^{spin-only} = 2.83\ \mu_B$) and indicates the presence of antiferromagnetic coupling between the $S = 3/2$ Cr^{III} ion and the $S = 1/2$ bridge in $[CrGa(tren)_2(CA^{sq,cat})]^{3+}$. The lack of any temperature dependence establishes that the magnitude of the splitting between the $S = 1$ and $S = 2$ states that result from spin exchange ($\Delta E = 4J$ for $\hat{H} = -2J\hat{S}_1 \cdot \hat{S}_2$, vide infra) greatly exceeds k_BT at 350 K. This observation is similar to what we[58] and others[89−93] have reported for other Cr^{III}−semiquinone complexes. DFT calculations carried out on $[Cr(tren)(3,6\text{-DTBSQ})]^{2+}$ reveal that the surprisingly strong interaction in these systems arises due to direct exchange between the SOMO of the semiquinone ligand and one of the d orbitals of the metal center;[85] Benelli et al. have studied related systems and were able to rationalize their data on the basis of the Tanabe formalism,[90] reaching essentially the same conclusions.[94,95] Although we have not carried out calculations on complex **4**, it is likely that an analogous

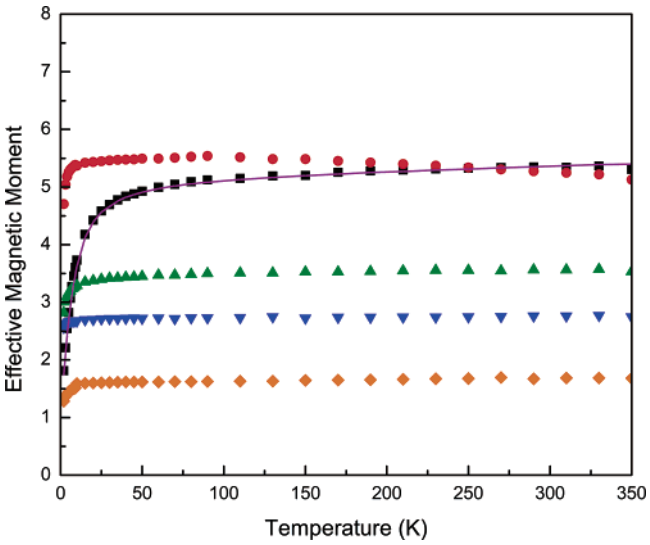

Figure 3. Plots of the effective magnetic moment versus temperature for complexes **2** (◆), **3** (▲),**4** (▼), **5** (■), and **6**(●) all acquired in the solid state. The solid line throuth the data for complex **5** corresponds to a fit using a Heisenberg spin Hamiltonian. See text for further details.

(88) The EPR spectrum of compound **2** also shows a structured rhombic feature near $g = 2$, indicative of an organic-based radical. The EPR properties of complex **2** along with other members of this series will be the subject of a separate report (Schrauben, J.; Guo, D.; McCusker, J. K. Manuscript in preparation).

(89) Buchanan, R. M.; Kessel, S. L.; Downs, H. H.; Pierpont, C. G.; Hendrickson, D. N. *J. Am. Chem. Soc.* **1978**, *100*, 7894.
(90) Benelli, C.; Dei, A.; Gatteschi, D.; Güdel, H. U.; Pardi, L. *Inorg. Chem.* **1989**, *28*, 3089.
(91) Chang, H.-C.; Ishii, T.; Kondo, M.; Kitagawa, S. *J. Chem. Soc. Dalton Trans.* **1999**, 2467.
(92) Shiren, K.; Tanaka, K. *Inorg. Chem.* **2002**, *41*, 5912.
(93) Chang, H.-C.; Mochizuki, K.; Kitagawa, S. *Inorg. Chem.* **2002**, *41*, 4444.
(94) Gondaira, K.; Tanabe, Y. *J. Phys. Soc. Jpn.* **1966**, *21*, 1527.
(95) McCarthy, P. J.; Güdel, H. U. *Coord. Chem. Rev.* **1988**, *88*, 69.

interaction exists in $[CrGa(tren)(CA^{sq,cat})]^{3+}$ between a π-symmetry d orbital on the Cr^{III} ion and the SOMO of $[CA^{sq,cat}]^{3-}$ to yield its antiferromagnetic ground state. Despite the magnitude of the interaction, our previous calculations[85] clearly showed that formulating the electronic structure of this class of compounds in terms of a spin-localized model in which the spin-coupled components retain distinct α- and β-spin polarizations is still appropriate.

The magnetic properties of complex **5** stand in contrast to the other members of the series in that the data show a pronounced temperature dependence. The value of μ_{eff} at room temperature of 5.32 μ_B is close to the spin-only value of 5.48 μ_B expected for two uncoupled $S = 3/2$ ions; however, the moment begins to drop below 100 K until reaching a value of $\mu_{eff} = 1.8\ \mu_B$ at 2 K. These data are qualitatively consistent with weak intramolecular antiferromagnetic coupling between the two Cr^{III} ions resulting in an $S = 0$ ground state. The data can be quantified using a simple Heisenberg spin Hamiltonian of the form

$$\mathbf{H} = -2J_{ij}\,\mathbf{S}_i\cdot\mathbf{S}_j \qquad (2)$$

where $\mathbf{S}_i$ and $\mathbf{S}_j$ are the single-ion spin operators for the ions involved in the exchange interaction, and J_{ij} is the scalar exchange integral which amounts to a coupling constant for that interaction. A fit of the data yields $J = -2\ cm^{-1}$ assuming a *g*-value of 2.0 and a contribution from temperature-independent paramagnetism of 4.0×10^{-4} cgsu. This small *J* value results in an overall spread of the four spin states within the ground spin manifold ($S = 0-3$) of only 24 cm^{-1}: this is responsible for the relatively low temperature at which the data asymptote toward the spin-only limit. The value of *J* that we measure is slightly smaller but still comparable to that of a related dinuclear Cr^{III} complex in which exchange is mediated by the dianionic form of chloranilate, $CA^{sq,sq}$.[55] It would appear from these results that diamagnetic configurations of chloranilate can propagate superexchange between the metals it bridges, but that this interaction is substantially weaker than the direct exchange available in complexes containing the $CA^{sq,cat}$ form of the ligand.[57]

The most complex system in terms of magnetic properties is compound **6**, which consists of two Cr^{III} ions bridged by $CA^{sq,cat}$. This three-spin system can be described using an elaborated form of eq 2,

$$\mathbf{H} = -2J(\mathbf{S_1}\cdot\mathbf{S_3} + \mathbf{S_2}\cdot\mathbf{S_3}) - 2J^*\mathbf{S_1}\cdot\mathbf{S_2} \qquad (3a)$$

where $\mathbf{S_3}$ represents the spin operator for the $CA^{sq,cat}$ bridge. The exchange integrals *J* and *J** in eq 3a quantify the $Cr^{III}-CA^{sq,cat}$ direct exchange and $Cr^{III}-Cr^{III}$ superexchange interactions, respectively. Defining the total spin of the system as $S_T = S_A + S_3$ (where $S_A = S_1 + S_2$), an operator-equivalent form of eq 3a can be readily derived (eq 3b)

$$\mathbf{H} = -J[\mathbf{S_T}^2 - \mathbf{S_A}^2 - \mathbf{S_3}^2] - J^*[\mathbf{S_A}^2 - \mathbf{S_1}^2 - \mathbf{S_2}^2] \qquad (3b)$$

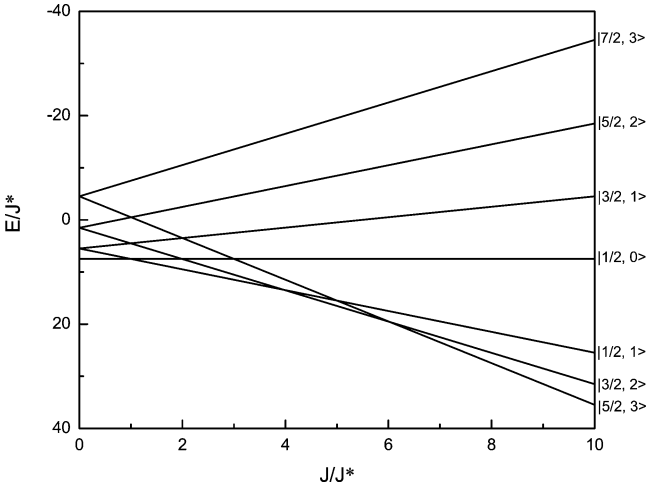

Figure 4. Plot of the eigenvalues from eq 3c calculated for $J < 0$ and $J^* < 0$ in units of J^*. States are labeled as $|S_T, S_A\rangle$, where S_T is the total spin and S_A is the corresponding value derived from coupling of the two Cr^{III} ions.

yielding the corresponding eigenvalue equation shown in eq 3c.

$$E = -J[S_T(S_T + 1) - S_A(S_A + 1) - S_3(S_3 + 1)] - J^*[S_A(S_A + 1) - S_1(S_1 + 1) - S_2(S_2 + 1)] \qquad (3c)$$

As with complex **4**, the effective magnetic moment data on $[Cr_2(tren)_2(CA^{sq,cat})]^{3+}$ show little temperature dependence, although there is a slight systematic decrease in effective moment that starts at ~100 K and continues as the temperature is increased to 350 K. The plateau at $\mu_{eff} = 5.60\ \mu_B$ that is maintained over the range of 10−100 K is consistent with a $S = 5/2$ ground state for this compound; the sharp drop below 10 K is likely due to zero-field splitting of the ground state. Our data are qualitatively similar to those reported by Dei et al. for the related complex $[Cr_2(CTH)_2(DHBQ)_2](ClO_4)_3$,[56] as well as $[Cr_2(CTH)_2(L)](PF_6)_3$ (where L is 5,5′-di-*tert*-butyl-3,3′,4,4′-tetrahydroxybiphenyl),[48] both of which also possess $S = 5/2$ ground states.

The lack of significant temperature dependence prohibits an accurate fit of the data for complex **6** to eq 3; however, we can still construct a reasonable semiquantitative energy level diagram for the ground-state spin manifold of this system on the basis of the data we have acquired on other members of this series. From the results obtained on $[CrGa(tren)_2(CA^{sq,cat})]^{3+}$ (complex **4**) and $[Cr_2(tren)_2(CA^{cat,cat})]^{2+}$ (complex **5**), it is reasonable to infer that both the $Cr^{III}-CA^{sq,cat}$ and $Cr^{III}-Cr^{III}$ interactions (*J* and *J**, respectively) in $[Cr_2(tren)_2(CA^{sq,cat})]^{3+}$ are antiferromagnetic in nature. A plot of the eigenvalues from eq 3c assuming that both *J* and *J** are negative is shown in Figure 4. This figure clearly illustrates that it is the relative (as opposed to the absolute) magnitude of the two coupling constants that has the most profound impact on the electronic structure of the molecule. In particular, we see that the ground state (corresponding to the bottom line for any given value of *J*/*J**) systematically shifts from $S_T = 1/2$ to 3/2 to 5/2 as *J* becomes larger in magnitude relative to *J**. Points along the *x* axis at which two lines intersect correspond to accidental degeneracies: the

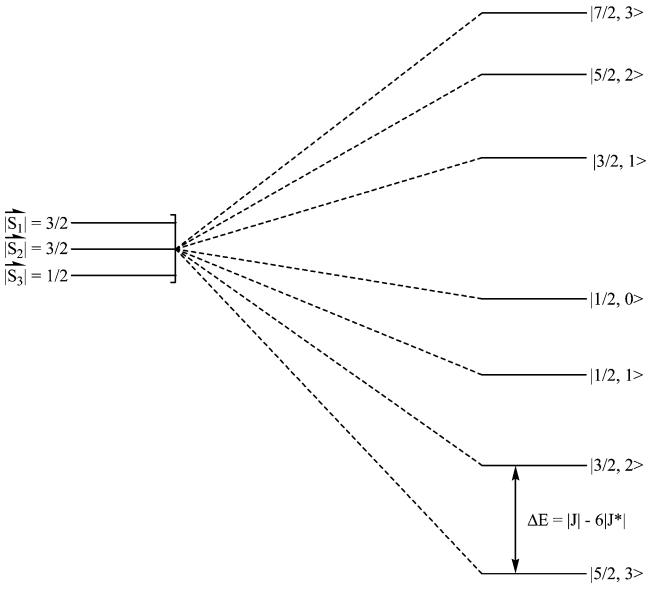

Figure 5. Energy level diagram for the ground-state spin manifold of $[Cr_2(tren)_2(CA^{sq,cat})]^{3+}$.

last of these occurs at $J/J^* = 6$, beyond which any further increase in this ratio serves to spread the spin manifold out energetically but does not cause any change in the relative ordering of states.

The data on complex **4** indicate that the direct exchange interaction quantified by J is on the order of several hundred wavenumbers. In contrast, the data on complex **5** affords a value for superexchange (albeit through a diamagnetic version of the bridge) of only -2 cm^{-1}. It is therefore reasonable to infer that the value of J/J^* in $[Cr_2(tren)_2(CA^{sq,cat})]^{3+}$ exceeds 6, giving rise to the energy level diagram shown in Figure 5. This model predicts a ground state for complex **6** of $S_T = 5/2$ ($S_A = 3$) with a first excited spin state of $S_T = 3/2$. This is consistent with the experimental data for complex **6** with regard to both the ground state and the slight decrease in effective moment in the range of 100−350 K. It must therefore be the case that the energy difference between these two states, which amounts to $|J| - 6|J^*|$, is sufficiently close to k_BT above 100 K to allow for some Boltzmann population of the $S_T = 3/2$ state.

It is significant to note that the ground state of complex **6** corresponds to one in which the relative spin polarization of the two Cr^{III} ions corresponds to a ferromagnetic alignment of the spins (i.e., $S_A = 3$) despite the fact that the $Cr^{III}-Cr^{III}$ coupling is antiferromagnetic. This is a classic manifestation of the form of spin frustration described by Hendrickson and co-workers in the context of a variety of other magnetic systems[1,96] wherein the dominance of one coupling pathway (in this case J, the $Cr^{III}-CA^{sq,cat}$ direct exchange) overwhelms another (J^*) such that the resulting spin polarization opposes the intrinsic nature of one of the two interactions.

B. Electronic Spectroscopy. Spin exchange interactions can arise whenever two (or more) paramagnetic moieties interact electronically. This situation can arise regardless of whether a molecule is in its ground state or an electronic excited state. Certain electronic transitions in spin-coupled systems may therefore involve radiative coupling between states modulated by spin exchange, resulting in substantive, fundamental changes in the spectroscopy of the compound. With the series of compounds we have developed, we have a unique opportunity to begin dissecting these contributions to the electronic spectroscopy of spin-coupled compounds.

Magnetically Dilute Systems. The simplest compounds to analyze are the Ga homobimetallic systems, complexes **1** and **2**. The electronic absorption spectra for both $[Ga_2(tren)_2(CA^{cat,cat})]^{2+}$ and $[Ga_2(tren)_2(CA^{sq,cat})]^{3+}$ in room-temperature fluid solution are shown in Figure 6. As expected, the spectrum of complex **1** is somewhat unremarkable. The single broad peak centered at $\lambda = 328$ nm ($\epsilon = 7400$ M^{-1} cm^{-1}) is easily assigned as a $\pi \rightarrow \pi^*$ absorption of the $CA^{cat,cat}$ group;[97,98] this assignment is further supported by the observation of a similar feature in the spectrum of H_4-CA. Upon oxidation of complex **1** to form $[Ga_2(tren)_2(CA^{sq,cat})]^{3+}$, a richly structured absorption feature is observed in the mid-visible. An advantage of incorporating Ga^{III} into these complexes is the lack of any charge-transfer bands associated with this ion in the spectral region we are considering. Therefore, this feature, which we also observe for H_3CA in basic solution and in complexes **4** and **6** (vide infra), correspond to absorptions endemic to the $CA^{sq,cat}$ ligand. Analogous patterns have been reported for a number of 1,4-benzosemiquinones in this same spectral region.[99]

The degree of structure evident in the spectrum of complex **2** is remarkable considering that these data were acquired in

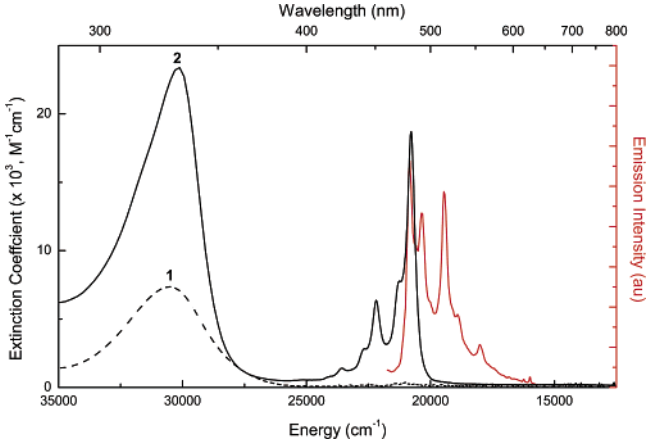

Figure 6. Ground-state absorption spectra of complexes **1** (dashed line) and **2** (black line), along with the emission spectrum of complex **2** acquired in a butyronitrile/propionitrile glass (9:2) at 90 K (red line).

(96) (a) McCusker, J. K.; Christmas, C. A.; Hagen, P. M.; Chadha, R. K.; Harvey, D. F.; Hendrickson, D. N. *J. Am. Chem. Soc.* **1991**, *113*, 6114. (b) McCusker, J. K.; Schmitt, E. A.; Hendrickson, D. N. In *Magnetic Molecular Materials*; Gatteschi, D., Kahn, O., Miller, J. S., Palacio, F., Eds.; Kluwer Academic Publishers: Dordrecht, The Netherlands, 1991; pp 297−319. (c) McCusker, J. K.; Vincent, J. B.; Schmitt, E. A.; Mino, M. L.; Shin, K.; Coggin, D. K.; Hagen, P. M.; Huffman, J. C.; Christou, G.; Hendrickson, D. N. *J. Am. Chem. Soc.* **1991**, *113*, 3012. (d) Squire, R. C.; Aubin, S. M. J.; Folting, K.; Streib, W. E.; Christou, G.; Hendrickson, D. N. *Inorg. Chem.* **1995**, *34*, 6463. (e) Libby, E.; McCusker, J. K.; Schmitt, E. A.; Folting, K.; Hendrickson, D. N.; Christou, G. *Inorg. Chem.* **1991**, *30*, 3486. (f) McCusker, J. K.; Jang, H. G.; Wang, S.; Christou, G.; Hendrickson, D. N. *Inorg. Chem.* **1992**, *31*, 1874.

(97) Platt, J. R. *J. Chem. Phys.* **1949**, *17*, 484.

(98) Vaillancourt, F. H.; Barbosa, C. J.; Spiro, T. G.; Bolin, J. T.; Blades, M. W.; Turner, R. F. B.; Eltis, L. D. *J. Am. Chem. Soc.* **2002**, *124*, 2485.

Table 4. Orbital Composition of Lowest-Energy Allowed Absorptions of $[CA^{sq,cat}]^{3-}$ Based on TD-DFT Calculations

			symmetry designation[c] (polarization)	
	f_{calcd}[a]	orbital transitions (c_i)[b]	C_{2v}	D_{2h}
Band I	0.038	52α → 56α (0.34)	$a_2 \rightarrow b_1$ (*y*-polarized)	$b_{1g} \rightarrow b_{3u}$ (*y*-polarized)
		53α → 57α (0.90)	$b_1 \rightarrow a_2$ (*y*-polarized)	$b_{2g} \rightarrow a_u$ (*y*-polarized)
		46*β* → 53*β* (0.21)	$a_2 \rightarrow b_1$ (*y*-polarized)	$a_u \rightarrow b_{2g}$ (*y*-polarized)
		52*β* → 56*β* (−0.26)	$a_2 \rightarrow b_1$ (*y*-polarized)	$b_{1g} \rightarrow b_{3u}$ (*y*-polarized)
Band II	0.11	51α → 54α (−0.19)	$a_1 \rightarrow a_1$ (*z*-polarized)	$b_{1u} \rightarrow a_g$ (*z*-polarized)
		52α → 57α (0.29)	$a_2 \rightarrow a_2$ (*z*-polarized)	$b_{1g} \rightarrow a_u$ (*z*-polarized)
		53α → 56α (−0.50)	$b_1 \rightarrow b_1$ (*z*-polarized)	$b_{2g} \rightarrow b_{3u}$ (*z*-polarized)
		50*β* → 53*β* (0.60)	$b_1 \rightarrow b_1$ (*z*-polarized)	$b_{3u} \rightarrow b_{2g}$ (*z*-polarized)
		51*β* → 54*β* (−0.47)	$a_1 \rightarrow a_1$ (*z*-polarized)	$b_{1u} \rightarrow a_g$ (*z*-polarized)

[a] Calculated oscillator strength. [b] c_i corresponds to the coefficient for the specific orbital transition in the multielectronic wavefunction for the calculated absorption. The contribution of each component to the total wavefunction is given by $c_i^2/\sum c_i^2$, where $\sum c_i^2 = 1$. [c] The coordinate system used for each point group symmetry is depicted in Chart 2.

room-temperature fluid solution. Two very clear vibronic progressions can be identified. The first, starting with what we presume to be the 0−0 transition at 480 nm ($\epsilon = 18700$ M^{-1} cm^{-1}), exhibits two discernible components at 450 nm ($\nu = 0 \rightarrow \nu' = 1$, $\epsilon = 6350$ M^{-1} cm^{-1}) and 424 nm ($\nu = 0 \rightarrow \nu' = 2$, $\epsilon = 1460$ M^{-1} cm^{-1}). The start of the second progression appears as a shoulder on the main peak at 470 nm with the $\nu = 0 \rightarrow \nu' = 1$ satellite showing up as a weak feature near 440 nm. The separation between the components for each of the two progressions is ∼1400 cm^{-1}: this compares quite favorably with a 1425 cm^{-1} band observed in the resonance Raman spectrum of $[Cr_2(tren)_2(CA^{sq,cat})]^{3+}$ (complex **6**, vide infra).[100] Also plotted in Figure 6 is the emission spectrum of $[Ga_2(tren)_2(CA^{sq,cat})]^{3+}$ obtained in a nitrile glass at 90 K. The spectrum is essentially a mirror image of the absorption profile. In particular, both of the vibronic progressions seen in absorption appear as fine structure in the low-temperature emission spectrum. The average energy spacing for both progressions in the emission profile is 1435 cm^{-1}: again this corresponds very well with the resonance Raman spectrum of complex **6** as well as a feature at 1436 cm^{-1} which we have assigned as a C−O stretch in the solution-phase ground-state infrared absorption spectrum of the complex **2**. Given the relatively small difference in vibrational spacings observed in the absorption and emission spectra, we can conclude that the ground- and excited-state configurations being sampled have very similar geometries with respect to the C−O bond coordinate.

Additional insight into the nature of this spectral feature was gleaned from time-dependent DFT calculations. These calculations were carried out on the uncomplexed $[CA^{sq,cat}]^{3-}$ ligand in the gas phase: the predicted transition energies are therefore not expected to stand in good agreement with the experimental spectrum of $[Ga_2(tren)_2(CA^{sq,cat})]^{3+}$ in solution. Nevertheless, the calculated wavefunctions can still provide useful information concerning the orbital character and polarization properties of electronic transitions within the chromophore. The first allowed absorption of $[CA^{sq,cat}]^{3-}$ manifests as two closely spaced transitions with calculated oscillator strengths of 0.038 and 0.11. The dominant contributions to these transitions along with their symmetries and predicted polarizations in the C_{2v} and D_{2h} point groups are listed in Table 4. Band I is dominated by a single transition, with 53α → 57α (Figure 7a) contributing >80% to the multielectronic wavefunction corresponding to this feature. In contrast, Band II reflects contributions from several origins, specifically 53α → 56α (∼25%), 50*β* → 53*β* (36%), and 51*β* → 54*β* (22%) (Figure 7b). Given how close in energy the two calculated transitions are and the relatively

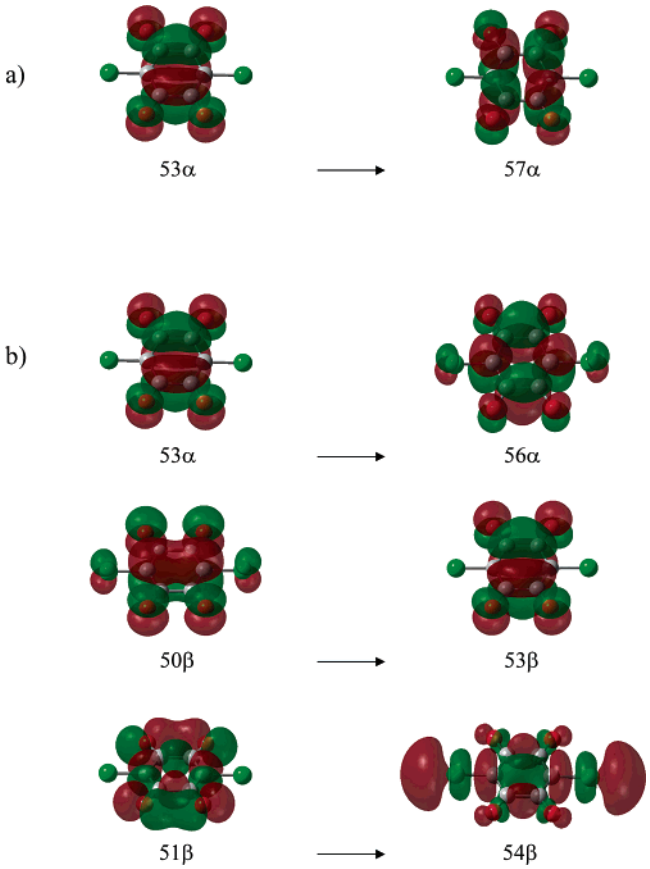

Figure 7. Drawings of the orbitals involved in the lowest-energy allowed transition(s) of $[CA^{sq,cat}]^{3-}$ based on a TD-DFT calculation. The atoms colored green correspond to the chlorine atoms of the ligand. (a) The 53α → 57α transition of Band I. (b) Transitions contributing to Band II. See Table 4 for further details.

(99) (a) Adams, G. E.; Michael, B. D. *Trans. Faraday Soc.* **1967**, *63*, 1171. (b) Land, E. J.; Simic, M.; Swallow, A. J. *Biochim. Biophys. Acta* **1971**, *226*, 239. (c) Johnston, R. F.; Holwerda, R. A. *Inorg. Chem.* **1985**, *24*, 153.

(100) Acquisition of the resonance Raman spectrum of $[Ga_2(tren)_2(CA^{sq,cat})]^{3+}$ was not possible due to emission from the sample.

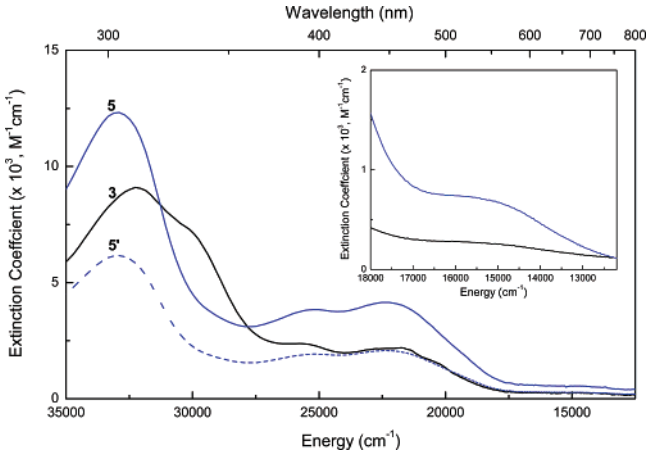

Figure 8. Room-temperature absorption spectra of complex **3** and complex **5** in acetonitrile solution. The blue dashed line (5′) corresponds to the spectrum of complex **5** divided by 2 and thus reflects the molar extinction coefficient of complex **5** per Cr^{III} ion.

small difference in their oscillator strengths, it is not clear whether Band I, Band II, or a combination of the two correlates with the feature observed in the spectrum of $[Ga_2(tren)_2(CA^{sq,cat})]^{3+}$. Nevertheless, the calculations do allow us to characterize the lowest energy absorption of $[CA^{sq,cat}]^{3-}$ as a $\pi^* \rightarrow \pi^*$ transition. Inspection of the initial- and final-state wavefunctions for all of these transitions reveals that the nature of the C−O bonding does not change appreciably between the initial and final states. This is qualitatively consistent with the similarity in fine structure between the absorption and emission spectra noted above.

Complex **3** is expected to possess absorption features characteristic of Cr^{III} unperturbed by spin exchange, and although the magnetic data on complex **5** clearly reveal that the two Cr^{III} ions are antiferromagnetically coupled, the coupling is apparently weak enough such that the absorptive properties of the compound can be understood as if the two ions were magnetically isolated. We will therefore consider the spectra of both of these complexes simultaneously. The spectra shown in Figure 8 reveal a number of transitions that are readily interpreted in terms of the well-known spectroscopy of six-coordinate Cr^{III}. The middle column of Figure 9 shows an energy level diagram for the low-lying ligand-field states of Cr^{III} assuming C_{2v} symmetry; the coordinate system we have chosen is depicted in Chart 2.[101] The lowest energy feature observed as a broad, weak band near 660 nm ($\epsilon \approx 300$ M^{-1} cm^{-1}) is assigned as the first spin-allowed d−d transition, namely, $^4B_2 \rightarrow (^4A_1, ^4A_2, ^4B_1)$; its measured intensity is likely augmented due to partial overlap with the more intense transition to the blue. This band is unusually low in energy for a $^4A_{2g} \rightarrow {}^4T_{2g}$-based transition and suggests that the $CA^{cat,cat}$ ligand is acting as a reasonably strong π-donor to the Cr^{III} ion. A second spin-allowed d−d absorption is often observed in the spectra of simple Cr^{III} complexes deriving from the $^4A_{2g} \rightarrow {}^4T_{1g}$ transition; however, this is obscured in complex **3** due to the presence of a more intense band centered near 450 nm.

(101) This figure corrects an error contained in a similar diagram in ref 58.

Chart 2

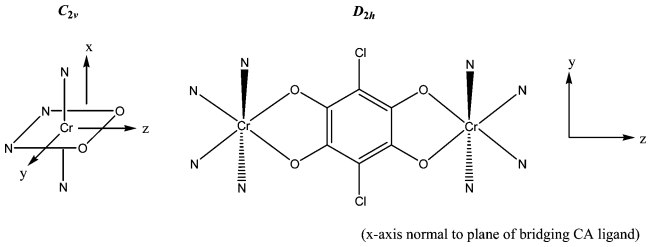

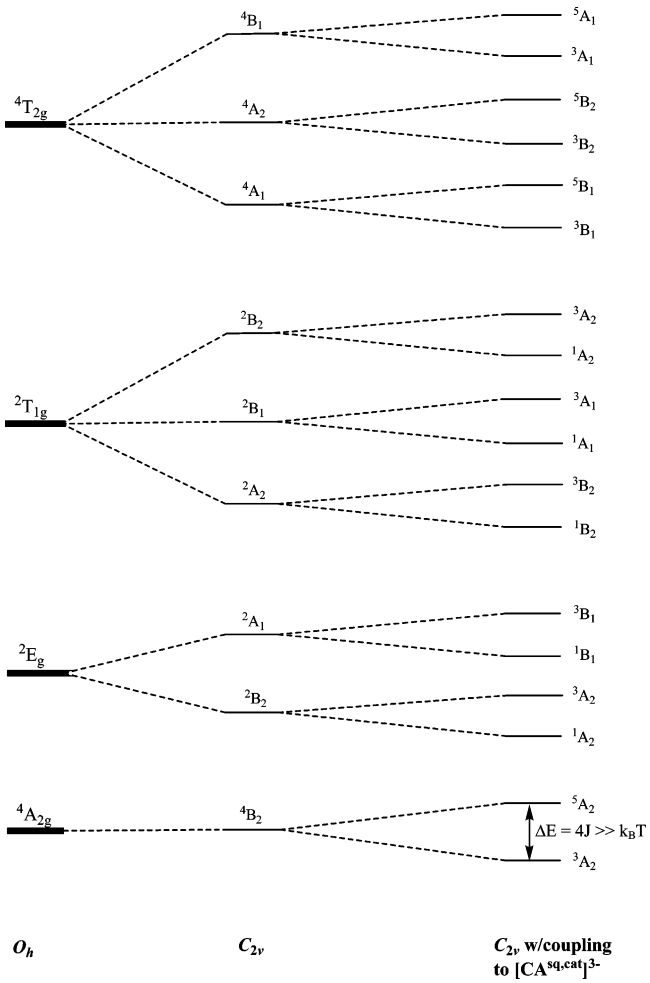

Figure 9. Qualitative energy level diagram for a Cr^{III}−quinone dyad. The first column indicates several of the lowest-lying ligand-field states present in a d^3 metal ion in O_h symmetry. The second column represents the splitting upon lowering the symmetry to C_{2v} and is appropriate for $[CrGa(tren)_2(CA^{cat,cat})]^{2+}$ in the coordinate system depicted in Chart 2 (the relative ordering of states derived from the T terms has been arbitrarily assigned). The third column represents splitting in C_{2v} when the unpaired spins of the metal couple to the $^2B_1$ term of $[CA^{sq,cat}]^{3-}$ in $[CrGa(tren)_2(CA^{sq,cat})]^{3+}$. The relative ordering of the spin-coupled excited states assumes antiferromagnetic exchange.

The extinction coefficient of this feature (ca. 2000 M^{-1} cm^{-1}) coupled with its absence in $[Ga_2(tren)_2(CA^{cat,cat})]^{2+}$ suggests that this is a charge-transfer band, most likely $^4B_2 \rightarrow {}^4$LMCT given the modest potential at which $CA^{cat,cat}$ is oxidized. The notion that this transition is associated with the Cr^{III} ion(s) is underscored by the fact that the intensity of the band correlates with the number of Cr^{III} ions present: this can be gleaned from the dashed line in Figure 8, a plot of the

spectrum of complex **5** per Cr^{III} ion. A second band is evident at 392 nm and is also tentatively assigned as a $^4B_2 \rightarrow {}^4$LMCT transition.

The highest energy transition near 310 nm is almost certainly the $CA^{cat,cat}$-localized transition observed in $[Ga_2(tren)_2(CA^{cat,cat})]^{2+}$; this assignment is supported by the fact that its intensity is underestimated in the plot of ϵ/Cr^{III}. It is interesting to note that this band is more asymmetric in the C_{2v}-symmetry complex **3** than what is observed for the D_{2h}-symmetric complex **5**: the pronounced shoulder near 330 nm for complex **3** is wholly absent in $[Cr_2(tren)_2(CA^{cat,cat})]^{2+}$. Here again, this feature does not correlate with the effective concentration of Cr^{III} as gauged by the ϵ/Cr^{III} plot, suggesting that it is a $CA^{cat,cat}$-localized transition. We cannot state with certainty whether this lower-energy feature transition is endemic to complex **3** or merely reflects splitting of the main band observed at higher energy in complex **5**. We tend to favor the latter explanation: it is not difficult to envision that merging of the two features at 310 and 330 nm in complex **3** would produce a band similar to that observed in complex **5**. This is supported by rough integrations of the features suggesting the overall oscillator strengths of both absorption envelopes are comparable. The origin of such a splitting in $[CrGa(tren)_2(CA^{cat,cat})]^{2+}$ is unclear but may reflect differences in the bonding of $CA^{cat,cat}$ to Cr^{III} versus Ga^{III}.

We were unable to detect any emission (at least out to 850 nm, the current limit of our apparatus) ascribable to $[CrGa(tren)_2(CA^{cat,cat})]^{2+}$ despite cooling the samples down to 10 K in a butyrlnitrile/propionitrile glass; similarly negative results were found for all of the Cr^{III}-containing compounds in this study. An extremely weak emission reminiscent of what we reported for $[Cr(tren)(3,6\text{-DTBCat})]^+$ at 90 K[58] was observed for several of the Cr^{III}-containing compounds. We examined this emissive component in detail in the case of complex **3** and found that its intensity was highly variable from sample to sample. In addition, the excitation profile of the emission did not track the absorption spectrum of the compound. We were ultimately able to trace our observations to the presence of a small amount of $Cr(tren)Cl_3$, which is used as a starting material for the synthesis of $[CrGa(tren)_2(CA^{cat,cat})]^{2+}$. This impurity was undetectable from either elemental analysis or ESI-MS results, an unfortunate testament to the extreme sensitivity of low-temperature emission spectroscopy. On the basis of these results and the fact that our previous synthetic procedure also utilized $Cr(tren)Cl_3$, we are forced to conclude that the emission we reported for $[Cr(tren)(3,6\text{-DTBCat})]^+$ was likely due to a similar impurity. Although beyond the scope of the present study, the absence of emission in these compounds is most likely the result of the very low energy at which the first quartet state excited-state is situated. This provides a facile nonradiative deactivation route for the ^2E state and quenching of the emission that might otherwise be expected for these Cr^{III} complexes.

Spin-Coupled Compounds. The electronic absorption spectra of complexes **4** and **6** are remarkably rich with features due to the individual constituents, as well as the coupling that exists among them. The most distinctive

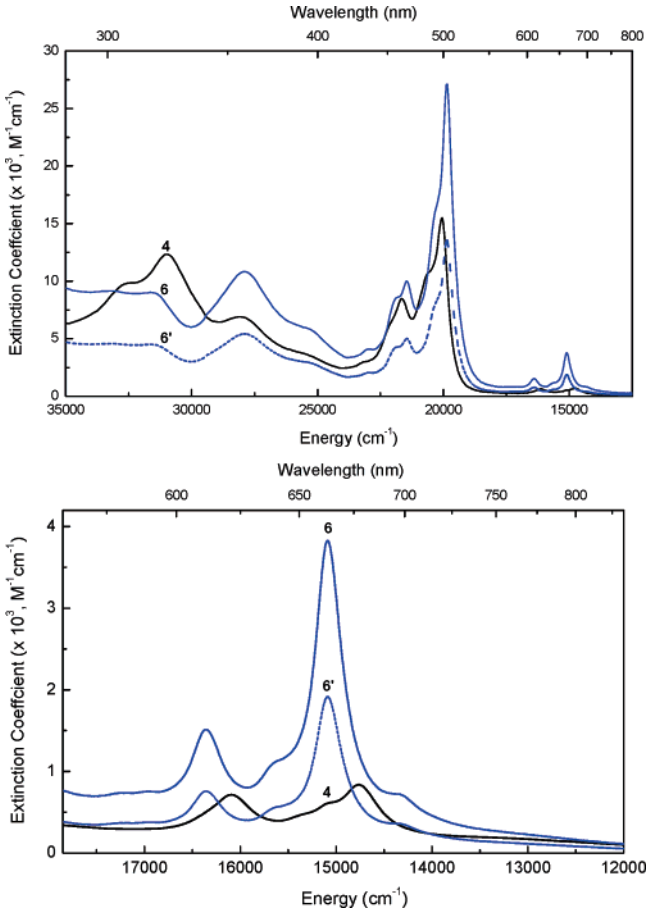

Figure 10. Room-temperature absorption spectra of complex **4** (black solid line) and complex **6** (blue solid line) in acetonitrile solution. The blue dashed line (6′) corresponds to the spectrum of complex **6** divided by 2 and thus reflects the molar extinction coefficient of complex **6** per Cr^{III} ion. The bottom panel is an expanded view of the low-energy region of the spectrum.

characteristic of the absorption spectrum of complex **4** is the presence of sharp, moderately intense bands in the region of 600−700 nm (Figure 10, lower panel). Similar features were noted by Dei and co-workers in the spectrum of $[Cr(CTH)(3,5\text{-DTBSQ})]^{2+}$ [90] and by us in the related complex $[Cr(tren)(3,6\text{-DTBSQ})]^{2+}$.[58] They do not appear in the spectrum of either $[Ga_2(tren)_2(CA^{sq,cat})]^{3+}$ (complex **2**, Figure 6) or $[CrGa(tren)_2(CA^{cat,cat})]^{2+}$ (complex **3**, Figure 8), indicating that these absorptions only arise when both Cr^{III} and $CA^{sq,cat}$ are present in the molecule. The sharpness of these absorptions is characteristic of an intraconfigurational transition; their location in the spectrum is consistent with transitions having $^4A_{2g} \rightarrow {}^2E_g$ and/or $^2T_{1g}$ parentage. These observations all point to their origin as exchange-enhanced ligand-field absorptions of the Cr^{III} ion.

An energy level diagram appropriate for complex **4** is shown in the right column of Figure 9. The term state designations for the various electronic states subject to spin exchange are easily obtained by taking the direct product of the irreducible representation for the SOMO of $CA^{sq,cat}$ (b_1) with the corresponding multielectronic term for the Cr^{III} ion (Figure 9, middle column). This yields the orbital symmetries; the spin multiplicities can then be added to produce the final array of states. Thus, the ground-state configuration for $[CrGa(tren)_2(CA^{sq,cat})]^{3+}$ is given by $^4B_2 \otimes {}^2B_1 \Rightarrow {}^3A_2 +$

$^5A_2$, with the $^3A_2$ state lying lowest due to the antiferromagnetic nature of the $Cr^{III}-CA^{sq,cat}$ interaction.

Coupling of the excited ^2E_g and $^2T_{1g}$ states of the Cr^{III} ion to the $[CA^{sq,cat}]^{3-}$ radical leads to the formation of new electronic states with differing spin. In the case of the low symmetry-split ^2E_g state, singlet and triplet states of A_2 and B_1 symmetry are produced; similar spin multiplicities for all three components of the $^2T_{1g}$ state are also realized.[102] Thus, in this region of the spectrum we can anticipate that spin exchange between the $[CA^{sq,cat}]^{3-}$ ligand and the doublet spin manifold of Cr^{III} will yield new absorption features due to the creation of new spin-allowed transitions. For the ^2E_g derived states, both the $^3A_2 \rightarrow {}^3A_2$ and $^3A_2 \rightarrow {}^3B_1$ transitions are symmetry-allowed in *z*- and *y*-polarization, respectively. The $^2T_{1g}$ term also leads to two allowed features, namely $^3A_2 \rightarrow {}^3B_2$ (*x*-polarized) and $^3A_2 \rightarrow {}^3A_2$ (*z*-polarized); the $^3A_2 \rightarrow {}^3A_1$ component is symmetry-forbidden. The effective relaxation of the spin selection rule is expected to lead to an enhancement in the intensity of transitions associated with these ligand-field states by $\sim 10^3$. The occurrence of exchange-modulated features across a number of different compounds suggests that enhanced radiative coupling to what was the doublet manifold of Cr^{III} is a defining characteristic of the spectroscopy of $Cr^{III}-$semiquinone complexes.

At present we can envision at least three possible assignments for these exchange-enhanced transitions: (1) Both features are associated with the ^2E_g state with 675 nm band assigned as $^3A_2 \rightarrow {}^3A_2$ and the higher-energy feature corresponding to the $^3A_2 \rightarrow {}^3B_1$ transition. Under this scenario, the energy separation of ~ 1300 cm^{-1} would correspond approximately to the low-symmetry ligand-field splitting of the ^2E_g state in C_{2v} symmetry. (2) The transition at 675 nm assigned as the 0−0 transition to the ^2E_g manifold, with the higher-energy band ascribed to the first vibronic component (i.e., $\nu = 0 \rightarrow \nu' = 1$). Within this assignment, the low-symmetry ligand-field splitting is presumed to be unresolved. (3) The lowest-energy band corresponds to $^3A_2 \rightarrow ({}^3A_2, {}^3B_1)$ from the ^2E_g state with the higher-energy band assigned as $^3A_2 \rightarrow ({}^3B_2, {}^3A_2)$ from the $^2T_{1g}$ term. As in case (2), this set of assignments presumes that the low-symmetry splitting of both O_h terms is unresolved.

In the absence of polarized absorption data, distinguishing among these three possibilities is difficult. Resonance Raman spectra acquired following excitation of complex **6** at ~ 650 nm did not reveal enhancement of any modes in the range of 1300 cm^{-1}, suggesting that option (2) described above is the least likely. It should be noted that although these bands are narrow, they are still significantly broader than what one typically observes for intraconfigurational transitions of magnetically dilute Cr^{III} ions. In addition, the molar extinction coefficients for both features are roughly a factor of 10 larger than relaxation of the spin selection rule alone would have afforded. Both of these attributes point to significant intensity stealing from the ligand-localized absorption in the mid-visible. Inspection of Table 4 reveals that the calculated transitions of $[CA^{sq,cat}]^{3-}$ are of the correct polarization to mix with both components of a $^4A_{2g} \rightarrow {}^2E_g$-based transition, with Band I able to mix with $^3A_2 \rightarrow {}^3B_1$ and the more intense Band II with $^3A_2 \rightarrow {}^3A_2$. Both Band I and Band II have contributions from the SOMO of $[CA^{sq,cat}]^{3-}$ (53α): since this orbital houses the unpaired electron of the chloranilate ligand involved in spin exchange with the Cr^{III} ion, there exists a facile mechanism for the type of intensity stealing we are suggesting. While this explains at least semiquantitatively the additional intensity observed for both of these exchange-enhanced features, it does not allow us to refine our assignments due to the fact that both the ^2E_g- and $^2T_{1g}$-derived states can, in principle, mix with the ligand-localized transitions of $[CA^{sq,cat}]^{3-}$. A more detailed analysis of these features is currently underway.

In addition to the appearance of new transitions arising due to spin exchange, several spectroscopic features endemic to the individual constituents are still retained. For example, inspection of the lower panel in Figure 10 reveals that the two exchange-enhanced bands just described are superimposed on a weaker, broad absorption feature. Comparison with the spectrum of complex **3** indicates that this is likely $^4A_{2g} \rightarrow {}^4T_{2g}$ in origin: in complex **4** this band is more formally designated as $^3A_2 \rightarrow ({}^3B_1, {}^3B_2)$, the third component of the symmetry-split $^4T_{2g}$ state being symmetry-forbidden. As noted by McCarthy and Güdel,[95] transitions that are spin-allowed in magnetically dilute compounds undergo little perturbation upon introduction of spin exchange. This appears to be the case in our system as well.

Transitions appearing at higher energies bear a striking resemblance to those already documented for $[Ga_2(tren)_2(CA^{sq,cat})]^{3+}$ and $[CrGa(tren)_2(CA^{cat,cat})]^{2+}$. In particular, the intense, structured absorption in the mid-visible that we[58] and others[90] had suggested might be due to a charge-transfer transition involving Cr^{III} in related compounds can now be confidently assigned as a ligand-localized transition associated with the $CA^{sq,cat}$ group by virtue of its similarity to the spectrum of $[Ga_2(tren)_2(CA^{sq,cat})]^{3+}$. The two distinct vibronic progressions noted in complex **2** are slightly broadened in complex **4** relative to complex **2** but are nevertheless clearly evident.

The pronounced feature near 360 nm ($\epsilon = 7000$ M^{-1} cm^{-1}) scales roughly with Cr^{III} ion concentration (dashed line) and is therefore assigned as a charge-transfer transition. Given the accessibility of both the $[CA^{cat,cat}]^{4-}$ and $[CA^{sq,sq}]^{2-}$ oxidation states of chloranilate and the fact that we were unable to observe signals in the compound's electrochemistry that could be ascribed to the Cr^{III} ion (either oxidative or reductive), it is unclear whether this absorption feature is MLCT or LMCT in nature. Last, the bands further to the ultraviolet are again the ligand-localized transitions that were observed in this same spectral region for $[Ga_2(tren)_2(CA^{sq,cat})]^{3+}$.

As with complex **4**, the spectrum of $[Cr_2(tren)_2(CA^{sq,cat})]^{3+}$ (complex **6**) contains features arising from the individual components of the molecule, as well as several due to coupling of the Cr^{III} ions to the bridging $CA^{sq,cat}$ group. The

(102) Although we have no direct information concerning excited-state exchange, it seems likely given the orbital interactions involved that coupling of the $CA^{sq,cat}$ ligand to the excited doublet and quartet ligand-field states of Cr^{III} will also be antiferromagnetic in nature.

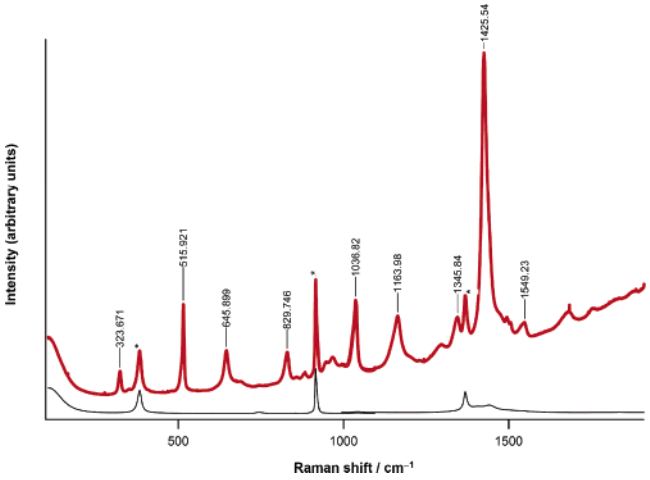

Figure 11. Resonance Raman spectrum of $[Cr_2(tren)_2(CA^{sq,cat})]^{3+}$ (complex **6**) in acetonitrile solution following excitation at 488 nm. Peaks marked with * correspond to background features arising from the solvent (black line).

structured band in the mid-visible is again due to the ligand-localized absorption of the $CA^{sq,cat}$ group. Figure 11 shows the resonance Raman spectrum of complex **6** following excitation at 488 nm. The strong enhancement of the 1425 cm^{-1} vibration—assigned as the C−O stretch of the $CA^{sq,cat}$ bridge—further supports our characterization of the fine structure associated with this absorption feature as a vibronic progression along this coordinate.

The change in the overall profile of this feature in complex **6** as compared to the heterobimetallic analogue deserves some comment. First, although the spectrum appears to have gained intensity in complex **6** relative to complex **4**, integration of the entire absorption envelope over the range 415−550 nm reveals that the oscillator strengths of this feature in both complexes are comparable. Thus, although the measured extinction coefficient at λ_{max} is indeed larger for complex **6** than complex **4**, the transition moment associated with this feature has not changed significantly upon incorporation of the second Cr^{III} ion. The second item of note is the enhanced prominance of the vibronic progression in complex **6**: the two closely spaced features near 465 nm in particular are much better resolved in the case of the homobimetallic analogue than for $[CrGa(tren)_2(CA^{sq,cat})]^{3+}$. These observations suggest that the ground- and excited-state potential energy surfaces (i.e., ΔQ) associated with this absorption are more nested in complex **6** versus complex **4**; this would account for the increased intensity in the $\nu = 0 \rightarrow \nu' = 0$ transition (λ_{max} = 505 nm), the slight loss in intensity in the higher vibronic components, as well as the overall increase in the resolution of the spectrum in the case of $[Cr_2(tren)_2(CA^{sq,cat})]^{3+}$. The reason for the decrease in ΔQ upon replacing Ga^{III} for Cr^{III} in $[CrGa(tren)_2(CA^{sq,cat})]^{3+}$ is not altogether clear, though we speculate that it may reflect the more symmetric nature of the interaction between the bridge and the metal ions in the case of $[Cr_2(tren)_2(CA^{sq,cat})]^{3+}$. This would allow for a more equal distribution of charge density across the ring, an effect that has been linked to decreases in excited-state distortions in other systems.[103]

Apart from the sharp, low-energy transitions to be discussed below, the only other features of note in the spectrum of complex **6** is the band near 360 nm—its near superposition with a similar feature in complex **4** coupled with its correlation with Cr^{III} concentration allows for an assignment as a charge-transfer band—as well as somewhat featureless absorptions further in the ultraviolet. These are likely the ligand-localized absorptions of $CA^{sq,cat}$ noted in complex **4** that is now partially obscured due to the increased contribution from the Cr^{III}-based CT band at 360 nm in $[Cr_2(tren)_2(CA^{sq,cat})]^{3+}$.

The most distinctive characteristic of the spectrum of complex **6** is again the presence of two sharp absorption bands in the red region of the spectrum. Given their overall profile and energetic proximity to the exchange-enhanced transitions identified for $[CrGa(tren)_2(CA^{sq,cat})]^{3+}$, a similar origin can be anticipated for these bands in $[Cr_2(tren)_2(CA^{sq,cat})]^{3+}$. Due to the presence of two Cr^{III} ions, however, the analysis of the electronic structure—in particular the excited electronic structure—is considerably more involved. The added complexity arises due to the fact that photon absorption can lead to two different but degenerate excited states, namely $[Cr^{III}* - CA^{sq,cat} - Cr^{III}]^{3+}$ and $[Cr^{III} - CA^{sq,cat} - Cr^{III}*]^{3+}$. As a number of groups have shown (most notably Güdel and co-workers[104]), this leads to a resonance condition which must be explicitly taken into account in order to properly interpret the spectroscopy of such systems. A detailed analysis along these lines for complex **6** will be the subject of a future report.

Concluding Comments

We have developed a series of compounds of the general form $[M^1M^2(tren)_2(CA^{n-})]^{m+}$ that has allowed us to clearly define physical and spectroscopic properties that arise solely due to the presence of spin exchange. The chloranilate anion, which forms a stable bridging chelate between two metal ions, was cycled between its trianionic $CA^{sq,cat}$ and tetranionic $CA^{cat,cat}$ states; systematic incorporation of Cr^{III} and/or Ga^{III} coupled with changes in the oxidation state of chloranilate yielded six compounds whose physical and photophysical properties have been thoroughly described. The electronic absorption spectra in particular revealed features characteristic of the individual components—for example, ligand-localized transitions associated with the bridging chloranilate—

(103) (a) Damrauer, N. H.; Boussie, T. R.; Devenney, M.; McCusker, J. K. *J. Am. Chem. Soc.* **1997**, *119*, 8253, and references therein. (b) Cuttell, D. G.; Kuang, S.-M.; Fanwick, P. E.; McMillin, D. R.; Walton, R. A. *J. Am. Chem. Soc.* **2002**, *124*, 6, and references therein. (c) Lyubimova, O. O.; Baranovskii, V. I. *J. Struct. Chem.* **2003**, 44, 728. (d) Benniston, A. C.; Chapman, G.; Harriman, A.; Mehrabi, M.; Sams, C. A. *Inorg. Chem.* **2004**, *43*, 4227. (e) Wang, Y. S.; Liu, S. X.; Pinto, M. R.; Dattelbaum, D. M.; Schoonover, J. R.; Schanze, K. S. *J. Phys. Chem. A* **2001**, *105*, 11118.

(104) (a) Decurtins, S.; Güdel, H. U. *Inorg. Chem.* **1982**, *21*, 3598. (b) Ferguson, J.; Güdel, H. U.; Krausz, E. R.; Guggenheim, H. J. *Mol. Phys.* **1974**, *28*, 893. (c) Schenker, R.; Weihe, H.; Güdel, H. U. *Inorg. Chem.* **1999**, *38*, 5593. (d) McCarthy, P. J.; Güdel, H. U. *Inorg. Chem.* **1984**, *23*, 880. (e) McCarthy, P. J.; Güdel, H. U. *Inorg. Chem.* **1986**, *25*, 838.

as well as new transitions that arise due to spin exchange among the various paramagnetic components. The ability to differentiate properties from these distinct origins was made possible by the synthetic methodology that provided clean access to the heterobimetallic members of the series. In addition, the redox-inert nature of the metal ions employed removed a level of ambiguity in terms of oxidation state assignment that can complicate analyses of these so-called non-innocent ligand systems.

Our ultimate goal with the development of these compounds is to understand the impact of spin exchange on the excited-state dynamics of molecules. Being able to determine which features arise due to spin exchange and which are intrinsic properties of the constituent components is critical for proper interpretation of those experiments. The systems we have described here represent an important step forward compared to the mononuclear complexes we described previously,[58,85] in that we can incorporate the spectroscopically silent Ga^{III} ion into our structural motif and maintain the overall integrity of molecule. This opens the door to a wide range of experiments that will allow us to further explore the interplay between electron exchange and the light-induced properties of molecules.

Acknowledgment. The authors are indebted to Professor Hans Güdel and Dr. Stefan Ochsenbein for helpful discussions. In addition, the authors would like to thank Dr. Denis Proshlyakov and Dr. Piotr Grzyska for the acquisition of the resonance Raman spectra and Richard J. Fehir, Jr. for carrying out the DFT calculations. This research was supported by the National Science Foundation (CHE-0213505 and CHE-0616340).

Supporting Information Available: Crystallographic data in cif format. This material is available free of charge via the Internet at http://pubs.acs.org.

IC070005Y